Geology, geochemistry and Sr-Nd constraints of selected metavolcanic rocks from the eastern boundary of the Saharan Metacraton, southern Sudan: A possible revision of the eastern boundary

M. A. Ibinoof [12], A. J. Bumby [2*], G.H. Grantham [3], E. M. Abdelrahman [4] and P. G. Eriksson [2] and P. J. le Roux [5]

[1] Department of Geology, Faculty of Petroleum and Minerals, University of Al Neelain, Sudan

[2] Department of Geology, Faculty of Natural and Agricultural Sciences, University of Pretoria, South Africa

[3] Council for Geoscience, Pretoria, South Africa

[4] Geological Research Authority, Khartoum, Sudan

[5] Department of Geological Sciences, Faculty of Science, University of Cape Town

Corresponding author:

E-mail: adam.bumby@up.ac.za

Cell phone: +27828150607

Department of Geology, Faculty of Natural and Agricultural Sciences, University of Pretoria, South Africa

Highlights

• Abutulu low-grade terrane lies west of the medium-grade gneiss of the Nuba Mountains, Sudan.
• This terrane is of Neoproterozoic age 778 ± 90 Ma.
• It is considered as remnants of a continental back-arc basin.
• The high-grade rocks of the Saharan Metacraton must lie further west.

Graphical abstract

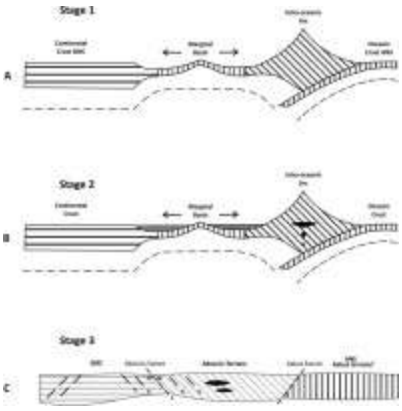

Abstract

Neoproterozoic, Pan-African low-grade metavolcanic rocks and associated mafic and ultramafic rocks of ophiolitic origin have long been identified within the pre-Neoproterozoic Saharan Metacraton (SMC). These low-grade rocks within generally high-grade (upper amphibolite facies) gneiss and schist have not yet been fully investigated, and their geological and geotectonic significance have been recognised only in a very few localities: (1) the Delgo – Atmur ophiolite and low-grade volcano-sedimentary belt, (2) the Rahib ophiolite and low-grade sedimentary fold and thrust belt, both in northern Sudan along the eastern boundary of the Saharan Metacraton and (3) the low-grade volcano-sedimentary rocks in the Central African Republic.

Dismembered and low-grade metamorphosed occurrences of mafic extrusive and intrusive and minor ultramafic rocks, grouped as the Arid unit, similar to those of the Arabian Nubian Shield (ANS), are reported here for the first time in the westernmost part of the Nuba Mountains, southeastern Sudan. These occurrences are interpreted to represent part of an ophiolite sequence with a lower cumulate layer composed of layered gabbro and minor cumulate hornblendite and a

top layer of thick massive gabbro, pillowed basalt and basaltic andesite. The Arid unit is structurally underlain by basaltic-andesite and andesite and a metasedimentary sequence identified as turbidite and both grouped as the Abutulu unit. All of the rocks are slightly sheared, deformed and metamorphosed under low-grade greenschist facies to epidote amphibolite sub-facies. New geochemical and Sr-Nd isotope data reveal that the low-grade metavolcanic rocks of the westernmost Nuba Mountains represent a Neoproterozoic oceanic arc/back-arc assemblage. The massive gabbro and pillowed basalt of the Arid unit show the geochemical characteristics of HFSE-depleted tholeiitic basalt while the co-genetic and more evolved meta-andesite of Abutulu unit show a calc-alkaline signature. Both units display a REE pattern characterized by LILE enrichment indicating formation in an arc/back-arc environment. This arc was active at around 778±90 Ma (Sm-Nd 12 WR isochron) that is similar in age to the arc magmatism in the ANS. The close interval between the TDM Nd model age (average of 10 metavolcanic samples is 814 Ma) and the crystallization age (778±90 Ma) is indicative of little or no involvement of older material. The western Nuba Mountains metavolcanic rocks have εNd values of +5.9 at 778 Ma (average of 12 samples) indicating a depleted mantle source similar to that of the ANS (published range from +6.5 to +8.4). The ε Nd values of the metavolcanic rocks are different from previously published ages of high-grade basement rocks that occupy the area west of the Kabus suture and east of Abutulu (+2.2 and +3.5 for the Rashad and Abbassyia).

It is proposed that the metavolcanic and associated plutonic mafic rocks represent a unique Neoproterozoic entity named the Abutulu terrane that developed in a marginal back-arc basin west of the medium-grade gneiss of the Nuba Mountains. If the Abutulu terrane is included as a part of the ANS, then the eastern boundary of the SMC is adjacent to the western edge of the ANS along the Abutulu suture.

1. Introduction

The Saharan Metacraton (SMC) (Fig. 1) is dominated by high- to medium-grade gneiss, metasedimentary rocks, migmatite and pockets of granulite (Abdelsalam et al, 2002). These units are intruded by numerous foliated granitoid rocks which usually grade into migmatite and granitic gneiss. Mineral assemblages are typical of amphibolite facies metamorphism (Vail, 1971; Schandelmeier et al., 1987; Harms et al., 1990; Abdel Rahman et al., 1990; El Ageed and El Rabaa, 1975; Abdelsalam and Dawoud, 1991; Abdelsalam et al., 2002; Küster and Liégeois, 2001; Küster et al., 2008).

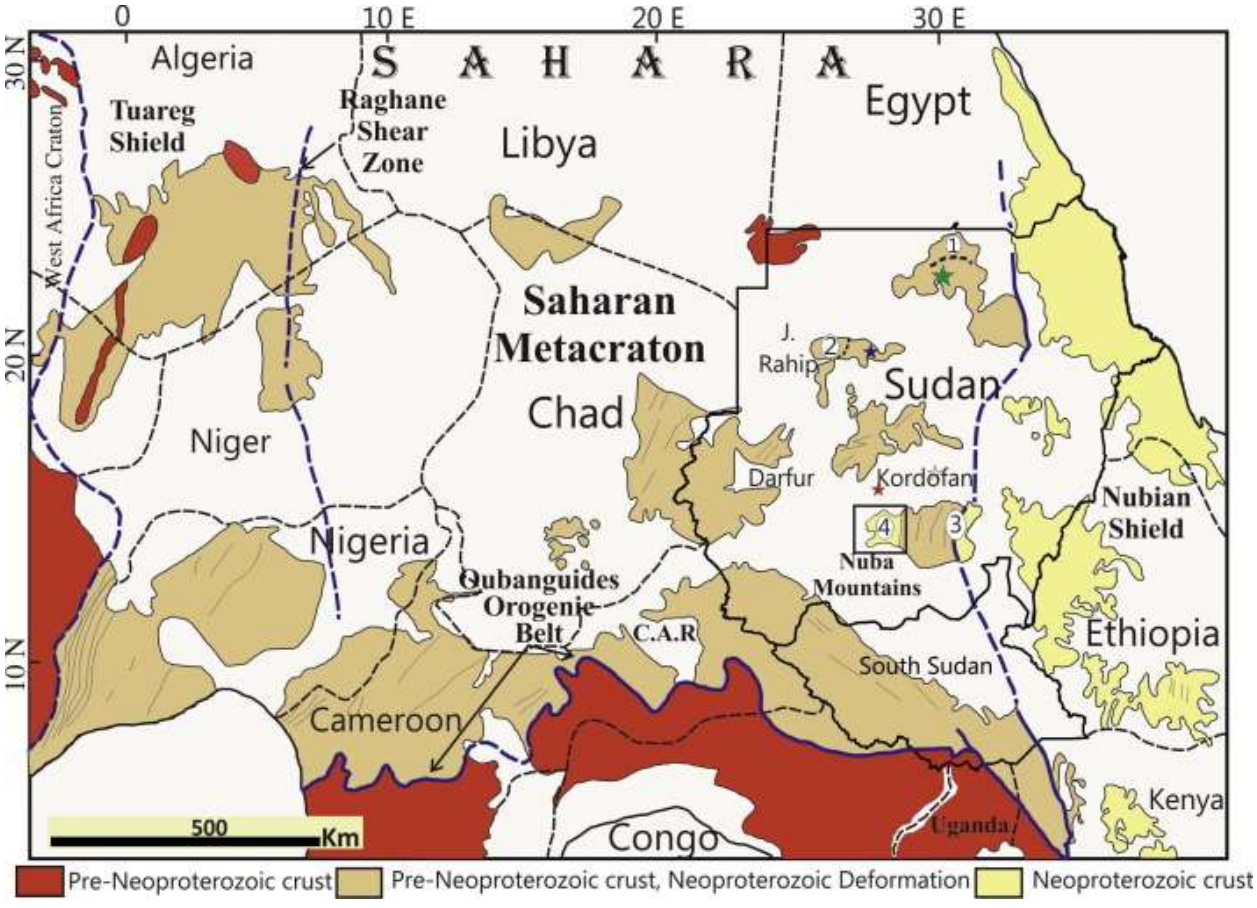

Fig. 1. Location map of the Saharan Metacraton (After Abdelsalam et al., 2002). White circles indicate localities mention in the text. 1 – Atmur-Delgo suture; 2 – Jebel Rahib fold and thrust belt; 3 – Kabus suture; 4 – Abutulu shear zone; Blue star – Wadi Hawar migmatite; Green star – Nubian Desert gneiss; Red star – El Obied muscovite granite.

The crust of the SMC was mostly remobilized during Neoproterozoic time. This remobilization of the SMC is in part due to collision between the continental tracts of East and West Gondwana at the end of the Pan-African orogeny between 630 and 610 Ma (Kröner and Stern, 2004). The term 'Pan-African' was firstly proposed by W Q Kennedy (1964) on the basis of an assessment of available Rb-Sr and K-Ar ages in Africa (Kröner and Stern, 2004). Events linked to the Pan-African orogeny not only exist in Africa but extend throughout the Gondwana continent and include the formation of a number of mobile belts surrounding the older cratons.

Low-grade volcano-sedimentary sequences similar to those of the Arabian Nubian Shield (ANS) are anomalous within the high grade gneiss of the region now known as the Saharan Metacraton (SMC), and was first mentioned by Vail (1983, 1985) who considered them as detached from the Arabian Nubian Shield. Other models to explain the low-grade metavolcanic rocks and ophiolite within the medium-grade gneiss are: (i) opening and closing of an aulacogen-like oceanic re-entrant (as suggested by Schandelmeier et al., 1990; Harms et al., 1994 and Denkler et al., 1994) to explain the WSW-trending Delgo – Atmur ophiolite and low-grade volcano-sedimentary belt and (ii) opening and closing of a Red Sea-like restricted oceanic basin without development of subduction zone and magmatic arcs (as suggested by Abdel Rahman et al., 1990 and Schandelmeier et al., 1990) for the formation of the N-trending Jebel Rahib ophiolite and low-grade sedimentary fold and thrust belt in central Sudan (Fig. 1). As a whole, the Saharan metacraton is a large Archean-Paleoproterozoic continental tract partly reactivated during the Neoproterozoic (Abdelsalam et al., 2002; Liégeois et al., 2013) following processes that remain poorly understood.

Mansour and Eskandar (1960) were the first to report the low-grade metavolcanic rocks in Abutulu in the westernmost Nuba Mountains in southern Sudan, ca. 300 km west of the Kabus

ophiolitic mélange (the eastern boundary of the SMC) (Fig. 1). They showed that the Abutulu iron ore mineralization is located within low-grade metavolcano-sedimentary rocks and they also reported the existence of glaucophane among the mineral assemblage of these rocks. Although low-grade volcano-sedimentary sequences within the SMC have been well documented, those from the western Nuba Mountains remain unstudied. Our aims were to: (1) verify the existence of such rock assemblages and to determine their extent and field relations, (2) identify the geotectonic affinity of these metavolcanic rocks, and (3) examine the validity of the models suggested for the occurrences of low-grade metavolcanic rocks that have been reported elsewhere in the SMC.

2. Geological framework of the Nuba Mountains

The Nuba Mountains region (NMR) is located in the southeast of Sudan (Fig. 2) and comprises an inlier of uplifted crystalline basement which is entirely surrounded by Mesozoic to Cenozoic sedimentary rocks filling several grabens (Sadig and Vail, 1986; Browne and Fairhead, 1983).

Early studies in the region by Vail; (1973), Shaddad et al. (1979), El Ageed and El Rabaa (1980) and Sadig and Vail, (1986) have divided the crystalline basement rocks into medium-grade gneiss and schist, low-grade metavolcano-sedimentary sequences and syn- to anorogenic granitoids. The latter have intruded both of the former units (Fig. 2). The presence of ultramafic rocks in the northeast of the Nuba Mountains was first described by El Ageed (1974) and these were identified as ophiolite by Hirdes and Brinkmann (1985), Brinkmann (1986) and Steiner (1987).

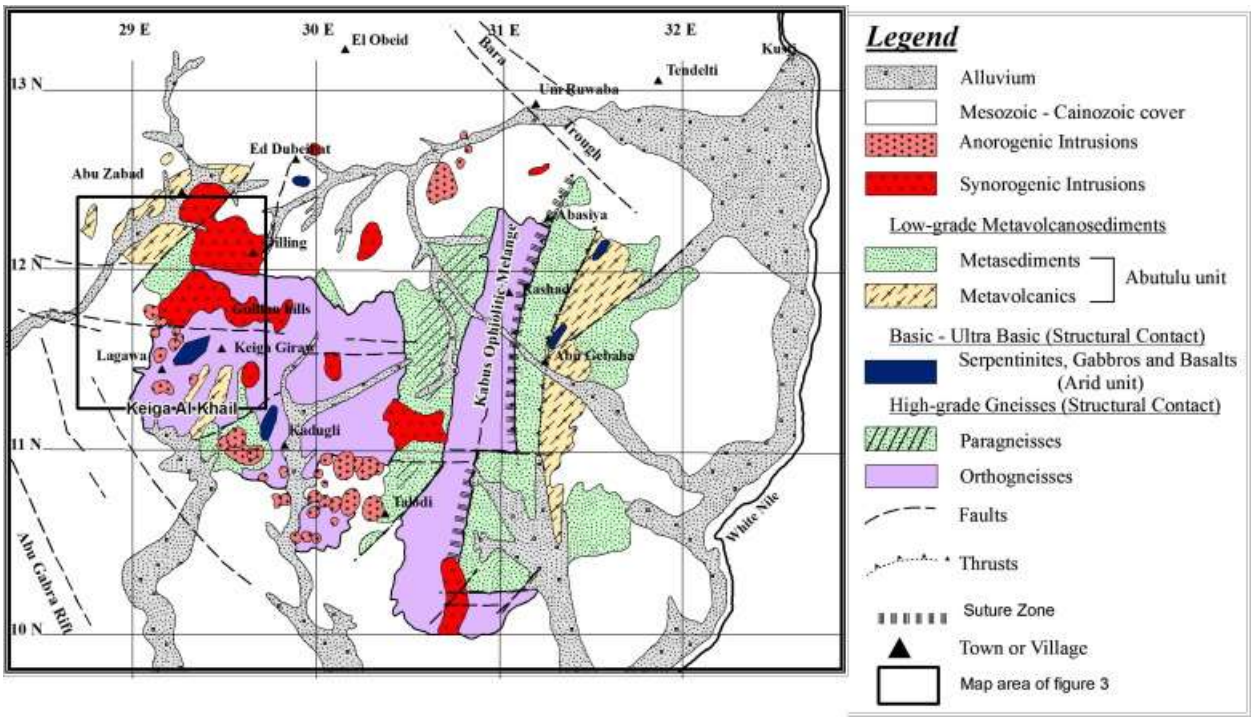

Fig. 2. Geological Map of the Nuba Mountains Region (modified after Sadig and Vail, 1986 and Abdelsalam and Dawoud, 1991).

Abdelsalam and Dawoud (1991) described these ophiolite fragments as a NNE-trending ophiolite-decorated suture zone. They introduced the name "Kabus ophiolitic mélange" and considered them to represent the eastern boundary of the SMC, which separates the high-grade gneiss in the west from the low-grade volcano-sedimentary sequence in the east (Fig. 1).

Although most of the region to the west of the Kabus ophiolitic mélange is underlain by amphibolite facies gneiss, the existence of low-grade greenschist facies metavolcanic and metasedimentary rocks has been reported at several localities in the western NMR (Sadig and Vail, 1986). Small bands of meta-andesite surrounded by granitic gneiss near Kega Al Khail (Fig. 2) have been reported by El Nadi (1984), while further to the north in the vicinity of Abu Zabad and around Abutulu (Fig. 2) similar metavolcanic rocks and low-grade phyllite are present (Mansour and Iskander, 1960 and Sadig and Vail, 1986 and references therein).

These low-grade metavolcanic and metasedimentary rocks are geographically associated with several mafic masses first reported by Lyns and Campbell Smith (1921), Vail (1973) and Sadig and Vail (1986). The mafic occurrences were originally interpreted by Vail (1973) as mafic intrusions that followed the metamorphism of the crystalline gneiss. However, this interpretation, which interpreted the rocks as mafic intrusions, has not been adopted by Vail in a more recent publication (Sadig and Vail, 1986), where the occurrences were mentioned within the volcano-sedimentary section, a unit that is suggested to be of ophiolitic origin compared to similar occurrences in the Ingassana and the Red Sea Hills regions of the ANS (Sadig and Vail, 1986).

3. Geology of the western Nuba Mountains

The area under consideration is situated in the westernmost NMR and bounded by latitudes 11° 9′ 0″ and 12 0′° 0″ N and longitudes 28° 32′ 0″ and 29° 40′ 0″ E covering an area of 11,910 km^2 (Fig. 3). Detailed geological mapping was carried out at the scale of 1:50000 utilizing ETM 7+ Landsat images.

Recent mapping has revealed six lithostratigraphic units: gneiss and migmatites, a metavolcano-sedimentary sequence, an extrusive and intrusive mafic belt, syn-orogenic granitoids, anorogenic granitoids, and Mesozoic sedimentary rocks. Most of the lithological units (except the anorogenic granitoids and Mesozoic sedimentary rocks) are traversed by an N- and NNE-regional structural trend (Fig. 2 & 3(A and B)).

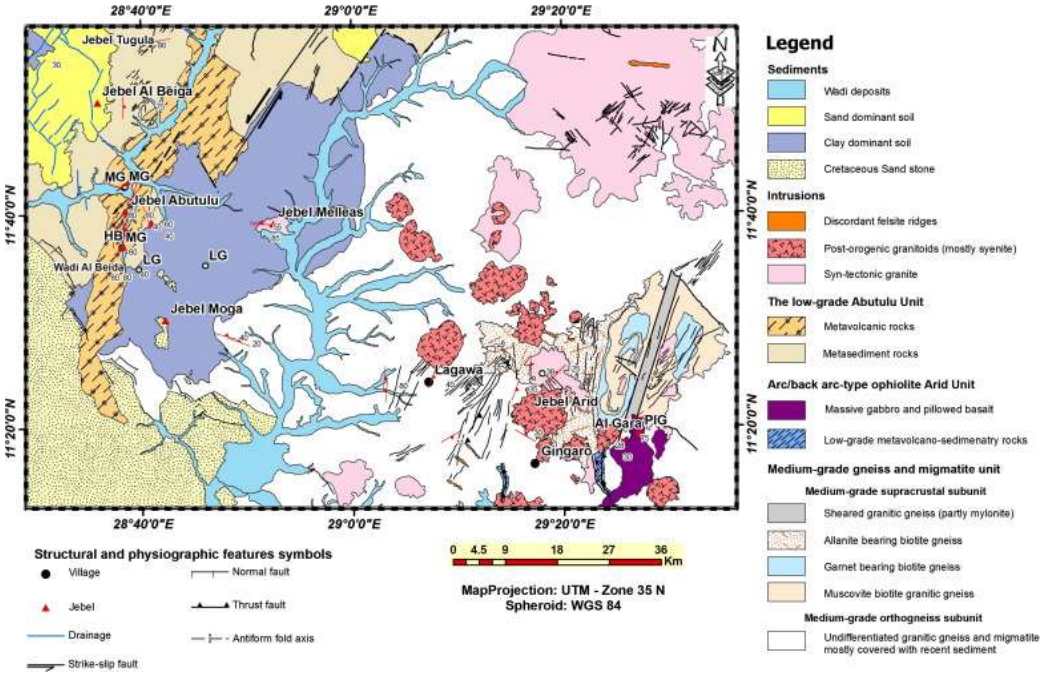

Fig. 3a. Geological map of the western Nuba Mountains. (MG) = Meta gabbro; (HB) = Hornblendite; and (LG) = Layered gabbro.

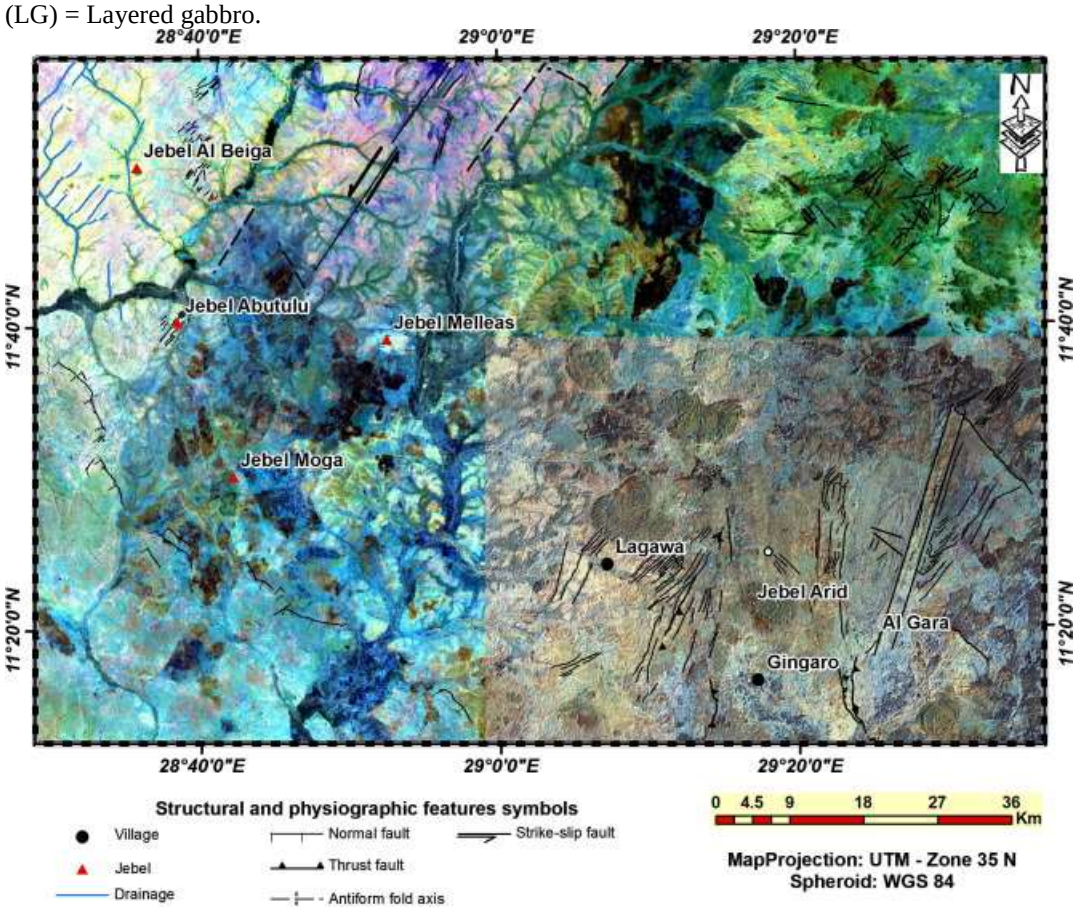

Fig. 3b. Landsat image of the western Nuba Mountains showing the scattered outcrops and the tonal contrast associated with the Abutulu shear zone.

3.1. Medium-grade gneiss and migmatite

3.1.1. Ortho-granitic and granodioritic gneiss

Gneissic rocks of granitic and granodioritic compositions occupy most of the eastern part and a portion of the centre of the study area (Fig. 3a). Sadig and Vail (1986), Mansour and Samuel (1957), Vail (1973), Brinkmann (1982) and Shaddad et al. (1979) have reported similar lithologies from areas in the eastern Nuba Mountains and in parts of the western Nuba Mountains. The gneiss crops out typically as low-lying features and in a few cases as hilly outcrops.

The granitic gneiss is composed of strained quartz, K-feldspar, plagioclase, biotite and variable amounts of muscovite. Secondary minerals include sericite, carbonate, epidote, zoisite and chlorite. Accessory minerals include zircon, apatite, titanite and opaque minerals. In the granodiorite gneiss, hornblende increases at the expense of biotite. K-feldspar augen gneiss (Fig. 4a) occurs only in the western part of the mapped area. The mineral assemblage of the granitic gneiss suggests amphibolite facies of regional metamorphism. Later retrograde metamorphism is indicated by the formation of chlorite after primary hornblende and biotite, and the formation of epidote after primary plagioclase. The homogeneity of the granitic and granodioritic gneiss composition suggests a magmatic origin.

The eastern contact of the medium-grade orthogneiss is reported to be against the Kabus ophiolitic mélange about 300 km to the east (Abdelsalam and Dawoud, 1991). Diffuse and gradational contacts separate the gneiss from the syn-orogenic granite of similar composition. Some of the previously mapped gneiss occurrences were found to be syn-orogenic granite containing xenoliths of the older gneiss unit (Fig. 4b) as seen in syn-orogenic granite just a few kilometers to the WSW of Lagawa. The contact against the low-grade volcano-sedimentary unit

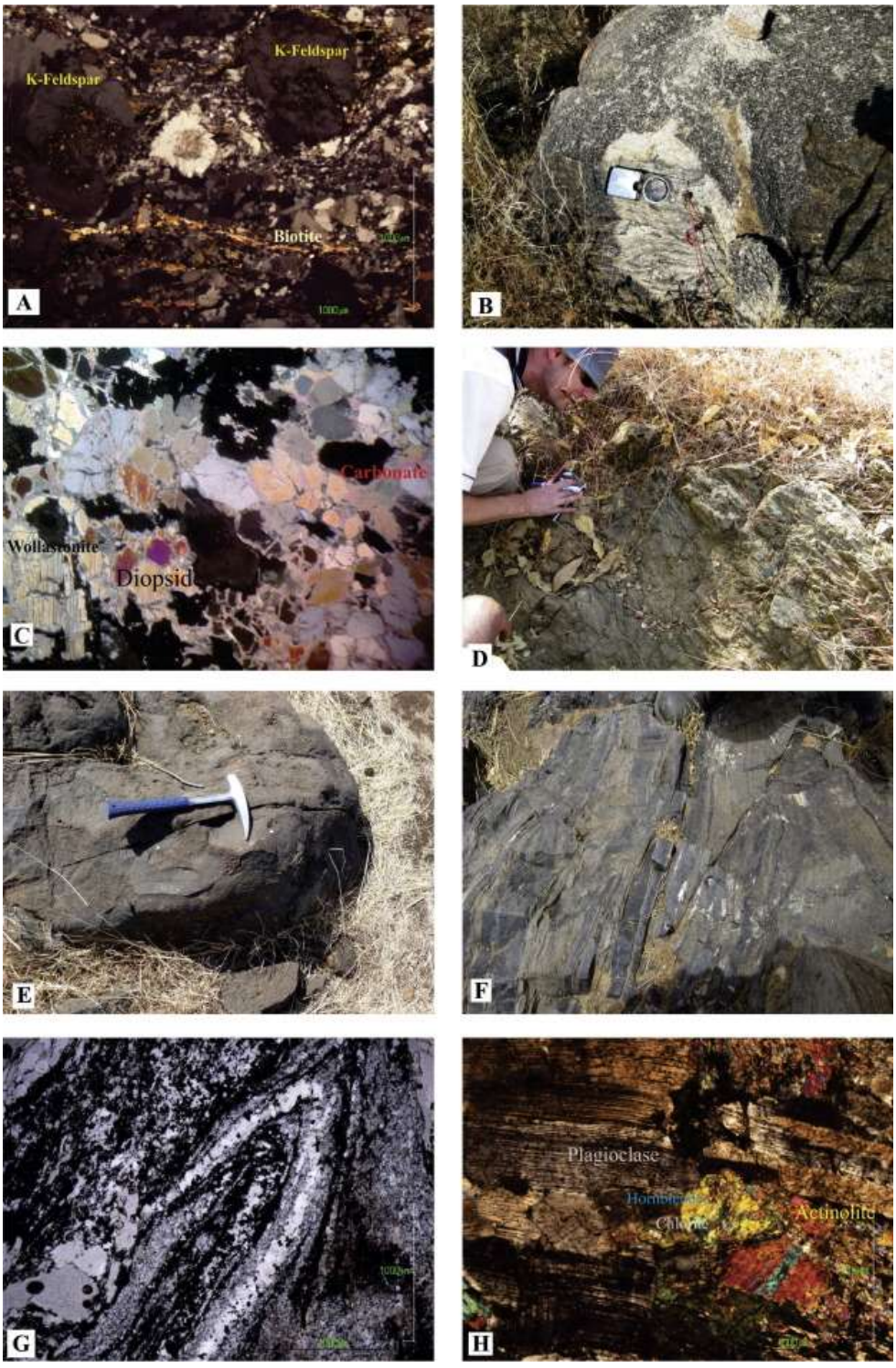

Fig. 4. (a) – the pre-tectonic feldspar porphyroblasts showing augen gneiss texture of medium-grade gneisses, (b) – well-banded gneissic xenoliths seen in syn-orogenic granite a few kilometers to the WSW of Lagawa (c) – medium-grade metamorphic minerals in Calc-silicate rock, (d) – layered gabbro along Wadi Tamba showing crude compositional layering, (e) – Photograph showing size and features of pillow basalt (f) – bedding in Tugula slate and (g) – micro-F1 folded bedding plane in Tugula (h) – Microphotograph showing the alteration of the layered cumulate gabbro.

to the west is demarcated by a steeply dipping sinistral shear zone. A sharp tonal contrast seen on the Landsat image (Fig. 3b) defines the contact. A sharp contact against the younger anorogenic granitoid intrusions is present and dykes of the younger intrusions are widely encountered in the vicinity of the intrusions. Detailed mapping of the younger intrusions and description of the nature of the contacts against the basement were given by Curtis and Brinkmann (1985).

3.1.2. Medium-grade metasedimentary rocks

A NNE-trending block of rocks ranging in composition from quartzo-feldspathic gneiss, quartzite, calc-silicate rocks (narrow bands), metavolcanic rocks and migmatite is structurally overlain by the orthogneiss unit (Fig. 3a). The paragneiss is made up of quartz, microcline, plagioclase, muscovite and minor biotite. Garnet and allanite exist in some samples. Accessory minerals are zircon and apatite. In the calc-silicate rock the main minerals are calcite, wollastonite, diopside, brucite and talc (Fig. 4c). Low-grade varieties only contain calcite and minor serpentine. The migmatitic mesosome is made up of hornblende, biotite and clinopyroxene and the leucosome is made up of plagioclase and quartz. Epidote, apatite and opaque minerals are seen in both of the previous varieties. The unit is intruded by both syn-orogenic and anorogenic granitoids. A contact aureole has been recorded adjacent to the impure marble.

The paragneiss is metamorphosed under amphibolite facies of regional metamorphism. The thermally metamorphosed impure limestone shows a mineral assemblage of slightly higher grade since the wollastonite is stable at higher temperature if fluid is H_2O rich. The rock association of quartzo-feldspathic gneiss, quartzite and marble is typical of a shallow water shelf depositional environment. This is possibly represents an insular shelf rather than the shelf of the SMC.

The metasedimentary rocks show a well-developed NNE-trending lineament (Fig. 3b). Thrust faults represent the boundary of a narrow strip of intercalated metasedimentary and metavolcanic rocks (Fig 3a).

The metasedimentary rocks are affected by a major south-plunging, easterly-verging asymmetrical antiform folded along a N-S to NNE-SSW trending axis (Fig. 3a).

3.2. Pillow basalt, massive gabbro and layered gabbro (Arid unit)

Dismembered low-lying fragments of basalt, massive gabbro and minor layered gabbro occupy a NNE – trending belt from around Kadugli in the south (Sadig and Vail, 1986) extending northwards to 60 km NW of Kadugli (Vail, 1973), north and northeast of Jebel Arid (this study) and 10 km SE of Ed Dubeibat (Lyns and Campbell Smith, 1921) (Fig. 2 and 3a). Only one very small exposure of hornblendite juxtaposes the layered gabbro occurrence along Wadi Al Beida (Fig. 3). Unfortunately, due to the poor outcrop (mostly hidden under thick cover of recent sediments) and the distance that separates the sub-units (ranging from hundreds of meters to tens of kilometers) no significant field relationships are observable. This renders it impossible to construct meaningful lithological log descriptions of the unit. The members of the Arid unit are presented below from bottom (layered gabbro) to top (basalt) based mainly on their textural relationships and available field.

3.2.1. Layered gabbro

The layered gabbro is greenish in colour with brown weathering surfaces, coarse-grained texture and crude compositional layering (Fig. 4d). It occurs in two exposures, one along the eastern boundary of the Arid metavolcanic rocks and the other one further east (Fig. 3a). Although there

is no obvious contact against the other members of the unit, the layered gabbro considered to be the lowest member within the mafic sequence based on its structure (layering). A N40E shear affects the layered gabbro, which is also shows intrafolial folds that plunge steeply to the SE.

The layered gabbro is composed of plagioclase and clinopyroxene in approximately equal amounts. Deformed plagioclase showing twisted lamellae and poikilitic texture is saussuritized to sodic plagioclase, epidote and sericite. The clinopyroxene is mostly retrograded to green hornblende and both are replaced by fibrous actinolite and chlorite. Apatite, titanite and iron oxides are the main accessory minerals. Epidote, zoisite, actinolite and chlorite are the main secondary minerals.

3.2.2. Massive gabbro

The massive gabbro crops out as boulders of medium to coarse-grained rock. It shows rare foliation and is locally slightly sheared. The massive gabbro is the dominant lithology among the mafic sequence. Its main outcrop is a sheet-like structure (as suggested from the gravity model of Sadig and Vail, 1986), in the south of a southerly plunging asymmetrical antiformal structure that exists east of Jebel Arid (Fig. 3a). The massive gabbro is made up mostly of approximately equal amounts of saussuritized calcic plagioclase and hornblende. Hornblende is retrograded after early clinopyroxene (augite). Uralitized clinopyroxene remains as relicts, partially replaced by green actinolite and chlorite. Orthopyroxene is evident in a few samples and is typically associated with olivine. The secondary minerals are epidote, zoisite, actinolite and chlorite while apatite and iron oxides are accessory minerals. The massive gabbro in two localities (Al Gara outcrop and east of Abutulu) is associated with pods and dykes of plagiogranite (Fig. 3a). The latter rock is light in colour and has a coarse-grained texture composed mainly of quartz and

sodic plagioclase and minor amount of biotite and iron oxide. Beside these two outcrops, numerous exposures of massive gabbro exist in the mapped area (Fig. 3a).

3.2.3. Basaltic lavas

Basaltic lava, rarely showing pillow structure, is underlain by massive gabbro northeast and east of Jebel Arid. The rocks are grayish green to dark green in colour and fine-grained in texture. The pillows are of oval shape and reach ~30 cm in size (Fig. 4e & 4f).

Petrographically, the rock shows weak to well developed foliation and is composed of mainly plagioclase, hornblende (up to 90%) and rare clinopyroxene. Secondary epidote and zoisite are also present together with the accessories titanite, chlorite, apatite and iron oxide. Subsequent alteration and possible retrogression is evident by the presence of calcic plagioclase saussuritized to sodic plagioclase, epidote and quartz, and minor replacement of hornblende by chlorite. The general mineral assemblage of the metabasite indicates low-grade metamorphism in the epidote-amphibolite sub-facies.

The structure of the above mentioned units is comparable to the structure of ophiolite successions as described by the Penrose conference (Anon conference, 1972; Coleman, 1977) as distinctive layered rock bodies including (from bottom to top) ultramafic tectonite, cumulate mafic – ultramafic rocks, non cumulate gabbros and sheeted dolerite dykes and mafic volcanic rock (basaltic pillow lava). This sequence is commonly overlain by pelagic sediment. In the succession under investigation the basal tectonite section is missing and the ultramafic cumulate is only represented by minor exposures of hornblendite.

3.3. Low-grade metavolcanic and metasedimentary rocks (Abutulu unit)

This group of rocks underlies the westernmost area of the Nuba Mountains and is mostly composed of poly-deformed and metamorphosed metavolcanic rocks (dominantly meta-andesite and sub-alkaline-basalt) and metasedimentary rocks (slate, phyllite, graphitic and mica quartzitic schist). The western boundary of the unit is hidden under the Quaternary sediments of south central Sudan (Fig. 3a). A tonal contrast on Landsat images coincides with the eastern boundary of the Abutulu unit separating it from the medium-grade gneisses and the covering clay soil (Fig. 3b).

Establishment of a stratigraphic column of the Abutulu unit is difficult due to the scattered and generally poor nature of the outcrop. The metasedimentary rocks of the Jebel Abutulu outcrop are bounded from both eastern and western sides by the metavolcanic rocks which may indicate intercalation between the two sub-units, like the general pattern observed in the Nuba Mountains. Both of the sub-units are sheared and folded along a general N30-50E strike but with more structural complexity in the metasedimentary rock.

The mica quartz schist is fine-grained, well-foliated and banded. Graphite schist is the dominant lithology among the metasedimentary rocks and crops out in several localities, from Kadugli in the south and northward thereof (Sadig and Vail, 1986 and references therein; this study). The main locality in the study area is Jebel Tugula in the northwest of the mapped area (Fig. 3a), where the primary sedimentary structure (bedding) can still be observed both at mesoscopic and microscopic scales (Fig. 4g & 4h).

The meta-andesite main outcrop is at Abutulu (Fig. 3b) where it appears as large and hard blocks of greenish grey colour with no developed joints. Other meta-andesite occurrences have only been seen as exposures along the dense network of drainage.

The metasedimentary rocks are fine-grained rocks and have a mineral assemblage of quartz, white mica, and graphite. Chlorite is the main secondary mineral, accompanied by biotite and epidote. Apatite and iron oxides are the accessory phases. Mansour and Iskander (1960) have reported a rare occurrence of glaucophane.

The metavolcanic rocks are made of porphyroblastic crystals of plagioclase in a finer groundmass of plagioclase, actinolite, chlorite, relict clinopyroxene and biotite. In many samples chlorite replaces all the mafic minerals. Epidote, zoisite, muscovite and quartz are the main secondary minerals. Apatite and opaques are the accessory minerals. Veinlets of carbonate and hydrothermal quartz are not uncommon. The general mineral assemblage indicates greenschist facies metamorphism.

4. Samples and analytical techniques

For the chemical study 39 samples, 24 from the Arid unit (gabbro and pillow basalt) and 15 from the Abutulu unit (meta-andesite and acidic metavolcanic), were selected for major, trace and rare earth element (REE) analysis. Major and trace element concentrations were determined by X-ray fluorescence using an ARL9400XP+ spectrometer in the XRD – XRF analytical facility of the Department of Geology, University of Pretoria, using fused glass beads for major elements and pressed powder pellets for the trace elements. The limits of detection for the major elements were better than 1%. A subgroup of 26 samples from both the Arid and Abutulu units was selected for high-precision determination of trace and REE element concentrations by induced coupled plasma mass spectrometry (ICP-MS) in the analytical facilities of the Department of Geological Sciences, University of Cape Town, South Africa.

The cumulate mafic rocks of the Abutulu unit were excluded from analysis because they were highly altered and deformed as described in section 3-2-1 and they had lost most of their original igneous characteristics.

5. Alteration and testing of element mobility

Previous petrographic examinations, as well as later determination of lost on ignition (LOI), (Tables 1 & 2) indicate that most of the samples have suffered from post-magmatic processes, including magma - sea-water interaction, regional metamorphism and later alteration. To evaluate the possibility of using the major elements we used the numerical index of alteration 100[(MgO + K2O)/ (MgO + K2O + CaO + Na2O)] of Hashiguchi et al., (1983), where indices of 36 ± 8 represent relatively unaltered samples. Most of our samples fall within the unaltered range (Table 1 & 2). Elements are known to behave differently under post-magmatic processes, (Hart, 1970; Polat et al., 1999; Humphris and Thompson, 1978; Mottl, 1983; Wilson, 1989). Variations in element behavior during weathering and hydrothermal alteration are commonly attributed to charge/radius ratio (ionic potential) (e.g. Pearce, 1996). Thus elements that form ions of low (<0.03 pm^{-1}) and high (>0.10 pm^{-1}) ionic potential tend to be preferentially removed in solution while elements that form ions of intermediate ionic potential (0.03-0.10 pm^{-1}) tend to stay in the solid product of weathering and so are relatively immobile; this is typically true even at greenschist-grade of metamorphism (Hastie et al., 2007). Thus the elements Zr, Hf, Nb, Ta, Y, Ti, Cr, REE except Eu and possibly La, Th, Ga and Sc are considered among the most immobile elements (Hastie et al., 2007; Pearce and Cann, 1973; Pearce, 2008; Shkol' nik et al., 2009).

However it's important for the mobility of each element to be tested since that even the immobile element may be mobilized under certain conditions such as, changes in the fluid composition, an

Table 1. List of major and trace element analyses for pillow basalts and massive gabbros of the Arid unit. The major oxides are calculated to 100% totals on an anhydrous basis as recommended by IUGS.

Oxides %	**Basaltic Pillow Lava**							**Massive Gabbro**												
Sample	**202 A**	**202 B**	**203 B**	**204**	**205**	**206 A**	**215**	**201**	**206 B**	**207**	**209**	**240 A**	**240 B**	**243**	**244**	**244 A**	**244 B**	**247**	**MG**	**GA**	**216**
SiO2	47.51	46.06	47.34	47.98	43.88	45.06	57.26	44.30	44.95	44.14	58.10	48.48	47.44	48.85	48.76	47.53	47.19	46.96	53.31	47.18	54.05
TiO2	1.46	1.34	1.40	1.47	1.50	1.56	0.71	1.33	1.44	1.27	2.72	0.77	0.68	0.78	0.87	0.57	0.74	0.98	0.56	0.25	0.64
Al2O3	17.37	17.18	17.74	17.47	16.88	18.95	15.02	18.70	20.19	20.87	14.36	13.87	16.37	17.46	20.37	17.89	18.19	18.86	14.98	13.97	17.44
Fe2O3	10.14	8.83	10.68	11.13	14.11	12.95	8.31	12.34	13.00	11.31	8.95	10.22	8.59	7.63	6.08	8.13	8.17	8.36	8.37	5.45	7.96
MnO	0.16	0.15	0.16	0.16	0.24	0.23	0.15	0.21	0.21	0.18	0.11	0.24	0.13	0.13	0.11	0.18	0.18	0.13	0.19	0.21	0.18
MgO	5.10	4.33	6.39	5.07	7.45	5.81	5.33	6.91	4.82	5.95	2.12	10.50	9.94	8.80	7.01	8.86	8.84	9.83	9.35	9.52	5.43
CaO	14.68	19.21	12.30	12.89	12.85	12.54	8.49	14.13	12.42	14.49	5.23	14.27	14.51	13.26	13.77	15.33	14.97	11.66	8.73	17.41	9.07
NaO2	2.37	1.45	2.68	2.50	0.67	1.55	3.20	0.66	1.84	0.83	3.22	0.28	0.70	1.35	1.69	0.13	0.14	1.78	3.03	1.75	3.60
K2O	0.31	0.14	0.50	0.45	1.06	0.43	0.31	0.43	0.37	0.31	3.46	0.29	0.15	0.41	0.29	0.11	0.16	0.33	0.21	0.15	0.32
P2O5	0.25	0.24	0.21	0.24	0.05	0.15	0.12	0.02	0.19	0.02	1.11	0.12	0.06	0.07	0.09	0.23	0.11	0.12	0.11	0.00	0.07
LOI	0.66	1.07	0.58	0.63	1.32	0.76	1.10	0.98	0.57	0.63	0.62	0.96	1.43	1.27	0.96	1.05	1.31	0.99	1.17	4.10	1.26
Total	100.00	100.00	100.00	100.00	100.00	100.00	100.00	100.00	100.00	100.00	100.00	100.00	100.00	100.00	100.00	100.00	100.00	100.00	100.00	100.00	100.00
Sc	35.1	31.0	31.1	32.6	45.1	32.8	18.8	45.1	18.8	31.2	8.7	55.2	23.7	36.3	34.4	35.0	31.7	51.1	15.6	61.3	33.9
V	225	207	217	226	409	360	152	409	198	321	82	288	163	202	232	214	194	270	112	200	193
Cr	243	200	156	221	94.2	30.4	267	94	12	45	21	241	387	923	275	266	935	280	907	774	187
Co	36.6	35.4	30.4	34.8	43.6	34.4	22.1	43.6	38.0	30.6	12.5	48.8	38.4	34.2	21.8	23.2	25.1	40.9	31.8	30.8	20.2
Ni	98.6	133	67.8	83.5	10.9	0	89.8	10.9	0.0	2.6	5.3	70.2	25.7	9.4	38.0	40.5	10.5	44.1	186.2	46.4	23.3
Cu	65.8	109	22.2	28.5	20.2	23.6	26.1	20.2	58.6	71.4	23.7	5.8	21.3	7.3	6.7	12.5	8.9	25.7	80.0	7.2	17.4
Zn	108	73.7	126	156	110	106	63.5	110	103	90	249	192	63	63	73	78	60	66	83	62	68.5
Rb	1.76	2.68	3.02	2.99	34.4	8.81	4.99	34.4	6.4	5.2	126.5	2.0	10.5	15.9	5.0	5.2	14.9	6.6	7.8	4.1	3.95
Sr	624	711	748	901	422	601	371	422	612	599	613	286	316	289	232	241	355	418	325	235	320
Y	27.1	25.2	24.5	27.2	12.2	13.2	29.7	12.2	9.5	8.3	32.9	13.2	15.5	16.7	18.9	21.4	18.8	16.3	20.6	13.6	16.8
Zr	21.7	33.7	19.3	19.5	11.8	11.1	62.9	11.8	7.1	10.6	231	13.4	14.2	51.6	40.3	37.8	58.9	32.9	97.8	22.7	30.7
Nb	2.82	2.56	2.47	2.73	0.71	1.22	3.66	0.7	0.9	0.8	27.5	2.9	1.0	3.1	4.2	3.5	3.1	2.7	4.3	2.0	1.23
Ba	95.1	56.4	227	147	150	117	59.9	149.6	98.2	84.6	1503	78.4	46.3	69.9	33.8	35.2	62.9	45.3	58.0	63.0	131
Hf	1.08	1.28	1.16	1.07	0.59	0.58	1.77	0.6	0.4	0.5	5.4	0.6	0.6	NA	NA	NA	NA	NA	NA	NA	1.19
Ta	0.09	0.08	0.15	0.12	0.01	0	0.22	0.0	0.1	0.0	1.1	0.1	0.0	NA	NA	NA	NA	NA	NA	NA	0.06
Pb	16.6	6.33	5.76	3.11	5.37	4.09	5.10	5.4	3.3	3.4	28.1	2.8	3.2	3.0	3.0	7.1	3.0	3.0	7.7	6.4	5.94
Th	0.41	0.35	0.46	0.44	0.26	0.34	4.21	0.3	0.2	0.3	26.2	1.2	0.4	3.0	4.3	4.7	3.0	3.0	3.0	3.0	1.63
U	0.20	0.19	0.31	0.20	0.22	0.29	1.15	0.2	0.2	0.2	5.8	0.9	0.2	3.0	3.0	3.0	3.0	3.3	3.0	3.0	0.70
La	9.34	7.86	8.10	9.29	2.90	4.72	10.9	2.9	4.1	2.7	167.7	8.3	4.0	17.5	17.1	20.5	15.9	18.1	16.2	18.9	7.21
Ce	25.0	20.9	22.1	25.0	7.39	11.9	24.5	7.4	9.9	6.8	350.	18.9	10.7	4.9	4.9	4.9	4.9	4.9	4.9	4.9	20.1

Oxides %	Basaltic Pillow Lava							Massive Gabbro													
Sample	202 A	202 B	203 B	204	205	206 A	215	201	206 B	207	209	240 A	240 B	243	244	244 A	244 B	247	MG	GA	216
											9										
Pr	3.62	3.10	3.35	3.68	1.18	1.85	3.36	1.2	1.4	1.0	39.2	2.6	1.6	–	–	–	–	–	–	–	2.20
Nd	17.3	15.1	16.1	17.9	6.44	9.71	15.3	6.4	7.2	5.2	151.4	11.9	8.3	–	–	–	–	–	–	–	9.35
Sm	4.48	4.05	4.31	4.69	2.10	2.77	4.34	2.1	1.9	1.5	23.1	2.9	2.4	–	–	–	–	–	–	–	2.58
Eu	1.69	1.60	1.54	1.57	0.91	1.24	0.98	0.9	1.0	0.7	4.1	0.9	1.0	–	–	–	–	–	–	–	0.83
Tb	0.84	0.78	0.79	0.82	0.39	0.45	0.77	0.4	0.3	0.3	1.8	0.5	0.5	–	–	–	–	–	–	–	0.47
Gd	5.39	4.99	4.90	5.36	2.46	3.13	4.74	2.5	2.1	1.7	15.5	3.1	3.0	–	–	–	–	–	–	–	2.88
Dy	5.16	4.78	4.64	5.06	2.41	2.67	5.13	2.4	1.9	1.7	8.0	2.7	3.0	–	–	–	–	–	–	–	3.06
Ho	1.01	0.95	0.97	1.01	0.47	0.53	1.06	0.5	0.4	0.3	1.3	0.5	0.6	–	–	–	–	–	–	–	0.64
Er	2.92	2.70	2.70	2.90	1.32	1.43	3.22	1.3	1.1	0.9	3.1	1.4	1.7	–	–	–	–	–	–	–	1.89
Tm	0.40	0.37	0.40	0.41	0.18	0.19	0.47	0.2	0.1	0.1	0.4	0.2	0.2	–	–	–	–	–	–	–	0.29
Yb	2.54	2.37	2.37	2.58	1.11	1.17	3.12	1.1	0.9	0.8	2.1	1.3	1.5	–	–	–	–	–	–	–	1.82
Lu	0.37	0.34	0.38	0.38	0.16	0.17	0.46	4.1	4.8	3.3	6.1	2.9	4.2	–	–	–	–	–	–	–	–
La/Nb	3.32	3.08	3.28	3.40	4.07	3.86	2.98	1.4	3.0	2.0	12.5	6.9	3.3	–	–	–	–	–	–	–	5.86
Ce/Pb	1.51	3.30	3.83	8.05	1.37	2.91	4.80	3.3	4.3	3.3	4.8	3.1	6.0	–	–	–	–	–	–	–	3.38
Nb/U	13.81	13.45	8.04	13.58	3.28	4.18	3.18	1.4	2.1	1.8	7.3	2.8	1.7	–	–	–	–	–	-	—	1.76
La/Sm	2.09	1.94	1.88	1.98	1.38	1.71	2.51	0.3	0.3	0.3	0.2	0.2	0.3	–	–	–	–	–	–	–	2.80
Sm/Nd	0.26	0.27	0.27	0.26	0.33	0.28	0.28	4.1	4.8	3.3	6.1	2.9	4.2	–	–	–	–	–	–	–	0.28
A.I.	24.1	17.8	31.5	26.4	38.6	30.7	32.6	33.2	26.7	29.0	39.8	42.6	39.9	38.7	32.1	36.7	37.3	43.1	44.9	33.5	31.2

Table 2. List of major and trace element analyses for metavolcanic rocks of the Abutulu unit. The major oxides are calculated to 100% totals on an anhydrous basis as recommended by IUGS.

Metavolcanics													
SAMBLE	SK50	SK51	SK52	SK54	SK55	SK28	SK 218	SK 219	SK 254	SK 256Br	SK 257	SK 258	SK 257A
SiO2	60.70	42.91	51.66	46.94	52.68	46.49	57.73	53.02	54.45	63.11	59.73	50.43	61.64
TiO2	1.49	0.87	2.16	1.40	1.36	1.66	1.65	1.87	2.37	1.90	1.53	1.26	1.56
Al2O3	14.01	12.42	15.75	16.83	12.10	16.30	12.27	14.66	15.77	17.21	13.75	15.80	14.41
Fe2O3	5.51	15.30	15.11	9.08	11.97	11.17	15.76	14.52	10.95	8.16	13.08	11.08	10.08
MnO	0.07	0.22	0.09	0.18	0.28	0.16	0.07	0.09	0.09	0.09	0.15	0.18	0.12
MgO	2.57	8.45	3.41	5.61	7.85	8.15	3.38	4.31	3.33	0.78	3.27	4.28	2.13
CaO	5.28	17.41	2.79	8.28	9.71	11.81	1.48	2.07	3.75	0.24	0.75	5.16	1.23
Na2O	6.68	0.00	5.92	2.72	1.88	1.75	4.58	5.41	7.14	0.06	4.29	4.43	5.81
K2O	2.79	0.23	0.16	0.83	0.42	0.71	0.11	0.11	0.28	5.02	0.05	0.77	0.06
P2O5	0.25	0.20	0.54	0.30	0.39	0.12	0.29	0.32	0.53	0.47	0.61	0.24	0.63
LOI	0.65	1.97	2.40	7.84	1.34	1.68	2.69	3.63	1.34	2.96	2.79	6.37	2.32
Total	100.00	100.00	100.00	100.00	100.00	100.00	100.00	100.00	100.00	100.00	100.00	100.00	100.00
Sc	18.5	25.3	20.1	22.6	33.7	24.7	25.3	28.1	28.5	25.8	16.3	27.8	26.03
V	71	115	219	194	223	210	293	285	250	154	69	202	73

Metavolcanics													
SAMBLE	**SK50**	**SK51**	**SK52**	**SK54**	**SK55**	**SK28**	**SK 218**	**SK 219**	**SK 254**	**SK 256Br**	**SK 257**	**SK 258**	**SK 257A**
Cr	5	462	36	85	165	293	42	34	34	56	10	98	7
Co	9	4	22	19	37	39	13	12	12	11	32	18	27
Ni	0	16	9	34	58	10	9	13	5	19	24	13	3
Cu	31	21	12	8	19	12	27	9	13	22	126	7	50
Zn	28	62	54	100	120	95	45	55	47	28	67	94	61
Rb	14	3	1	10	9	16	1	1	2	84	1	14	3
Sr	64	394	63	496	682	324	54	63	74	41	59	157	71
Y	42	24	65	26	32	36	23	26	76	30	32	16	80
Zr	291	92	343	34	32	131	203	236	483	335	407	173	446
Nb	8	3	8	6	7	5	6	6	10	6	8	3	11
Ba	385	91	35	252	142	123	31	41	63	699	72	217	69
Hf	8	2	9	–	–	–	5	6	10	8	10	4	–
Ta	1	0	0	–	–	–	0	0	1	0	0	0	–
Pb	2	3	2	10	13	3	2	2	5	2	2	2	3
Th	6	4	8	3	4	3	4	4	9	7	7	4	4
U	4	3	4	3	5	3	2	2	4	3	3	2	3
La	31.0	21.9	17.1	–	–	–	12.7	8.9	23.1	41.6	39.2	16.2	31.8
Ce	54.0	56.4	44.3	–	–	–	34.9	30.6	57.1	81.8	86.1	38.5	123.5
Pr	7.0	8.0	6.5	–	–	–	5.3	5.3	8.2	12.5	12.1	5.0	–
Nd	29.0	34.4	30.3	–	–	–	24.7	26.4	39.0	53.9	53.2	22.4	–
Sm	6.9	7.2	9.3	–	–	–	6.1	7.2	11.1	11.1	11.4	5.5	–
Eu	1.7	1.5	2.2	–	–	–	1.3	1.4	2.4	2.2	2.1	1.5	–
Tb	1.1	0.8	1.7	–	–	–	0.7	0.9	2.1	1.1	1.2	0.7	–
Gd	7.0	6.1	11.0	–	–	–	5.4	6.4	13.4	8.9	9.7	5.2	–
Dy	7.0	4.6	11.3	–	–	–	4.4	5.0	13.1	5.7	5.8	3.2	–
Ho	1.4	0.9	2.3	–	–	–	0.9	1.1	2.6	1.1	1.2	0.6	–
Er	4.4	2.4	6.6	–	–	–	2.7	3.0	7.7	3.6	3.8	1.9	–
Tm	0.6	0.3	0.9	–	–	–	0.4	0.5	1.1	0.6	0.6	0.3	–
Yb	4.5	2.1	6.1	–	–	–	2.9	3.3	7.0	4.1	4.6	2.3	–
Lu	0.7	0.3	0.9	–	–	–	0.5	0.6	1.0	0.7	0.8	0.4	–
La/Nb	3.72	8.09	2.07	–	–	–	2.31	1.47	2.30	6.93	5.04	4.89	–
Ce/Pb	35.28	17.97	20.92	–	–	–	20.99	16.16	12.65	45.74	35.26	16.99	–
Nb/U	2.30	0.91	2.12	–	–	–	3.20	2.71	2.67	2.08	2.62	2.11	–
La/Sm	4.50	3.03	1.84	–	–	–	2.07	1.24	2.09	3.75	3.45	2.96	–
Sm/Nd	0.24	0.21	0.31	–	–	–	0.25	0.27	0.28	0.21	0.21	0.24	–
A.I.	30.9	33.3	29.1	36.9	41.7	39.5	36.6	37.2	24.9	95.1	39.7	34.5	23.8

increase in temperature and/or extremely high fluid throughput (e.g. Hastie et al., 2007; Hynes, 1980; McCulloch & Gamble, 1991; Pearce, 1996; Hill et al., 2000).

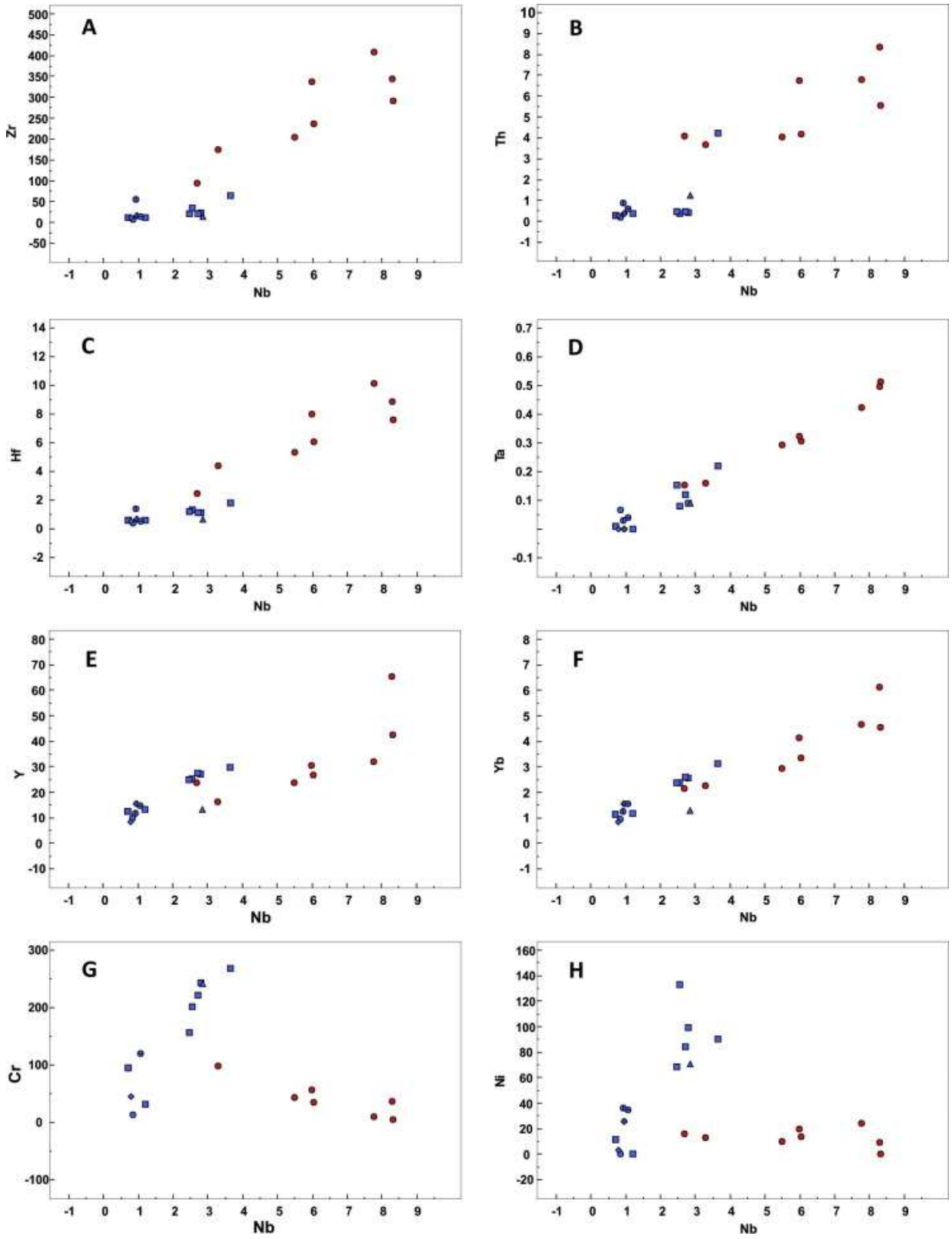

Fig. 5. Bivariate plotting of Zr, Th, Hf, Ta, Y, Yb, Cr and Ni vs Nb for samples of Arid and Abutulu units. Blue color rectangles are for the Arid unit basalt samples; Red color circles are for the Abutulu unit gabbro samples

In this study the method described by Cann (1970) is implemented in which an immobile element (Nb in this study) is plotted on the horizontal axis and the tested element on the vertical axis. If the elements are immobile and the samples are cogenetic the data should give trends with slope close to a straight line.

Plotting of Hf, Ta, Y and Yb for samples of Arid and Abutulu units (fig. 5a, b, c, d, e and f) provides slopes that are close to straight lines, suggesting the immobility of these elements and the cogenetic nature of the two units. Figures 5g and 5h are showing two trends with the Arid unit samples almost having vertical slope. We interpret these two trend features as possibly due to the accumulation of the minerals containing these two elements.

6. Major and trace element geochemistry

Although lithological, structural and spatial differences between the Arid and Abutulu units have been described in previous sections, the bivariate plotting of various elements from both units against their Nb contents (Fig. 5a to 5f) clearly suggests the cogenetic nature of the two units and that the variation between these units could be explained by intra-formation differentiation. Split of samples into two trends exhibited by Cr and Ni (Fig. 5G & 5H) is interpreted to result possibly from the accumulation of accessory minerals by the mafic Arid samples.

Thus we will deal with the geochemistry of the two units in a single section. However, each lithological group will be assigned a unique symbol and will be discussed in a separate sub-section for the sake of comparison.

6.1. Pillow Basalt

The pillowed basalts from the Arid unit shows limited variation in SiO_2 from 44.74% to 49.15%, (with one sample show higher content of 57.86%), TiO_2 from 0.72% to 1.58%, MgO from 4.43% to 7.6%, Fe_2O_3t from 8.39% to 14.38% and in K_2O from 0.14% to 1.08% (Table 1). The Mg# (= {100*Mg (Mg + 0.8FeOt)}) (Luhr, 1997) has low values that range from 36.3 to 41.2. These values are lower than those of primary lavas > 62 (Luhr, 1997; Kampunzu et al., 1998).

The lavas have high La/Nb (2.98 – 4.07), La/Sm (1.38 – 2.51), Sm/Nd (0.26 – 0.33) and low Nb/U (1.64 – 7.97), Ce/Pb (1.37 – 8.05) element ratios compared to those of extensional tectonic settings (e.g., in MORB and WPB including OIB and continental rift basalt emplaced far from any convergent margin {Sun & McDonough, 1989}). Instead, these values are similar to those of arc lava (Plank, 2005 and references therein).

The Zr/TiO_2 vs Nb/Y diagram (Fig. 6a) classifies the samples as sub-alkaline basalt, basaltic andesite and andesite. They also plot as island arc tholeiite basalt (with the exception of Sk215) in the Th vs Co classification diagram (Fig. 6b). The pillow lava clustered on the tholeiitic trend of the AFM diagram (Fig. 6c).

The MORB normalised multi-element spiderdiagram of major and trace elements shows features that are typical of subduction–related trace element features (fig. 7a) and similar to those of the Vanuatu arc (Peate et al., 1997). These features include enrichment of large-ion lithophile elements (LILE) relative to light rare earth elements (LREE) (e.g., Ba/La* ≈ 8.1) and enrichment in both LILE and LREE relative to high-field strength elements (HFSE) (e.g., Ba/Nb* ≈ 27.7; La/Nb* ≈ 3.2). The HFSEs, Hf and Zr are depleted relative to the LREEs, Nd and Sm. These features are common in arc lava and are attributed to the involvement of a sediment component

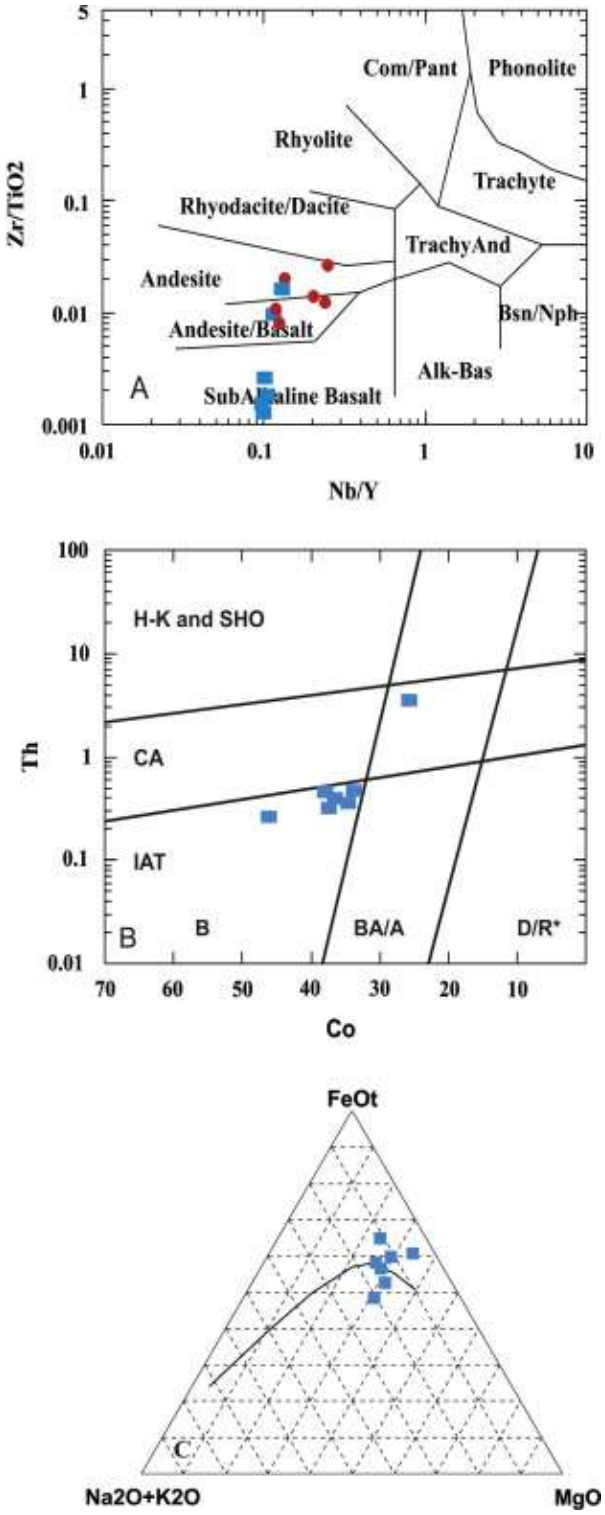

Fig. 6. (a) Zr/TiO2 vs Nb/Y diagram (after Winchester and Floyd, 1977) utilizing the classification of the samples as sub-alkaline basalt, (b) Th vs Co classification diagram which classifies Arid samples as island arc tholeiite and Abutulu samples as calc-alkaline basaltic andesite and andesite (after Hastie et al., 2007), (c) AFM diagram showing a tholeiitic trend for Arid samples and calc-alkaline trend for Abutulu samples (After Irvine and Baragar, 1971). Blue color rectangles are for the Arid unit basalt samples; Red color circles are for the Abutulu unit gabbro samples.

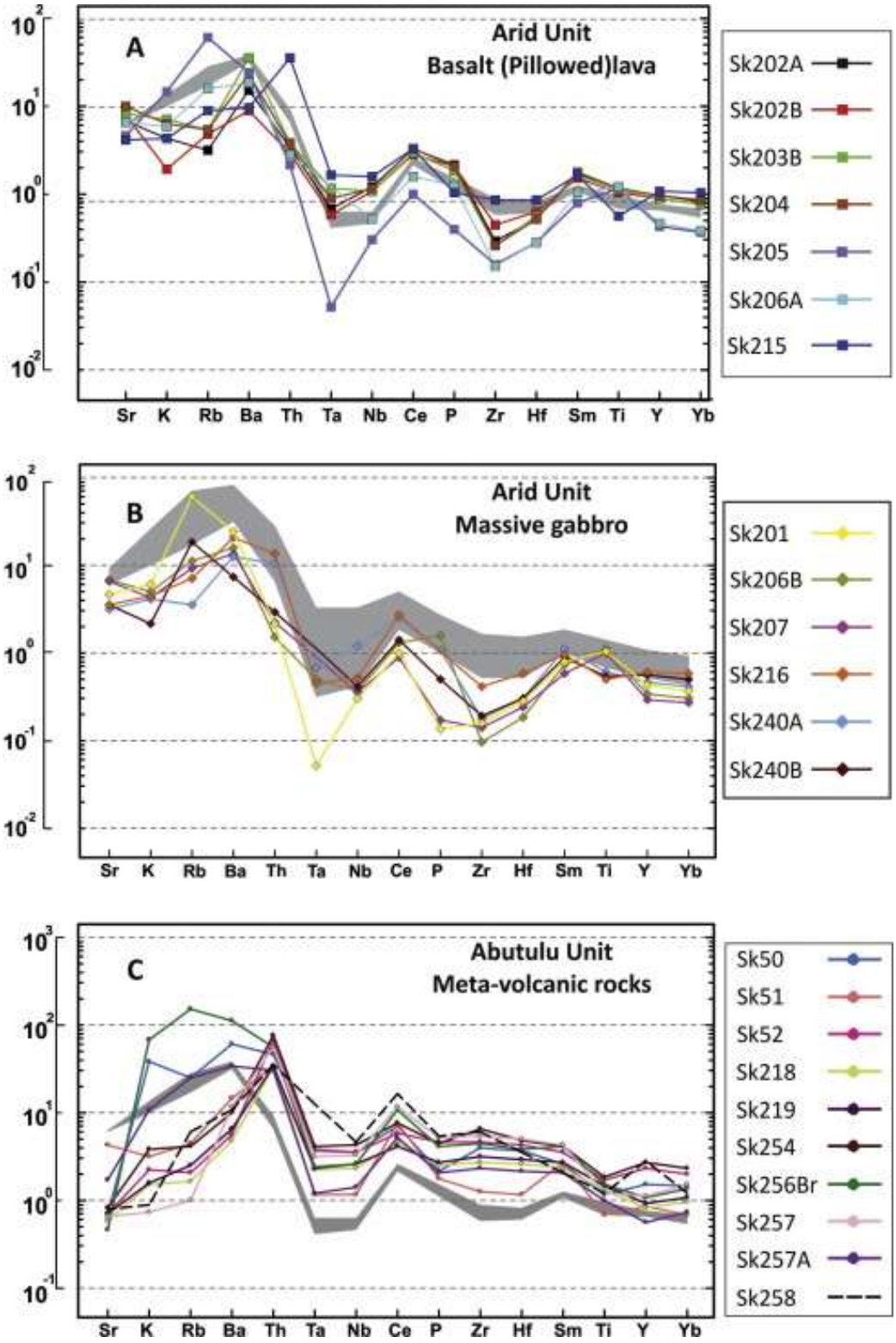

Fig. 7. MORB multi-element spider diagram of major and trace element showing features similar to those of suprasubduction zone ophiolites for (a) pillow basalts, (b) massive gabbros and (c) the meta-andesite. Normalized values are from Sun and McDonough (1989). The grey shaded area represent samples Vanuatu arc.

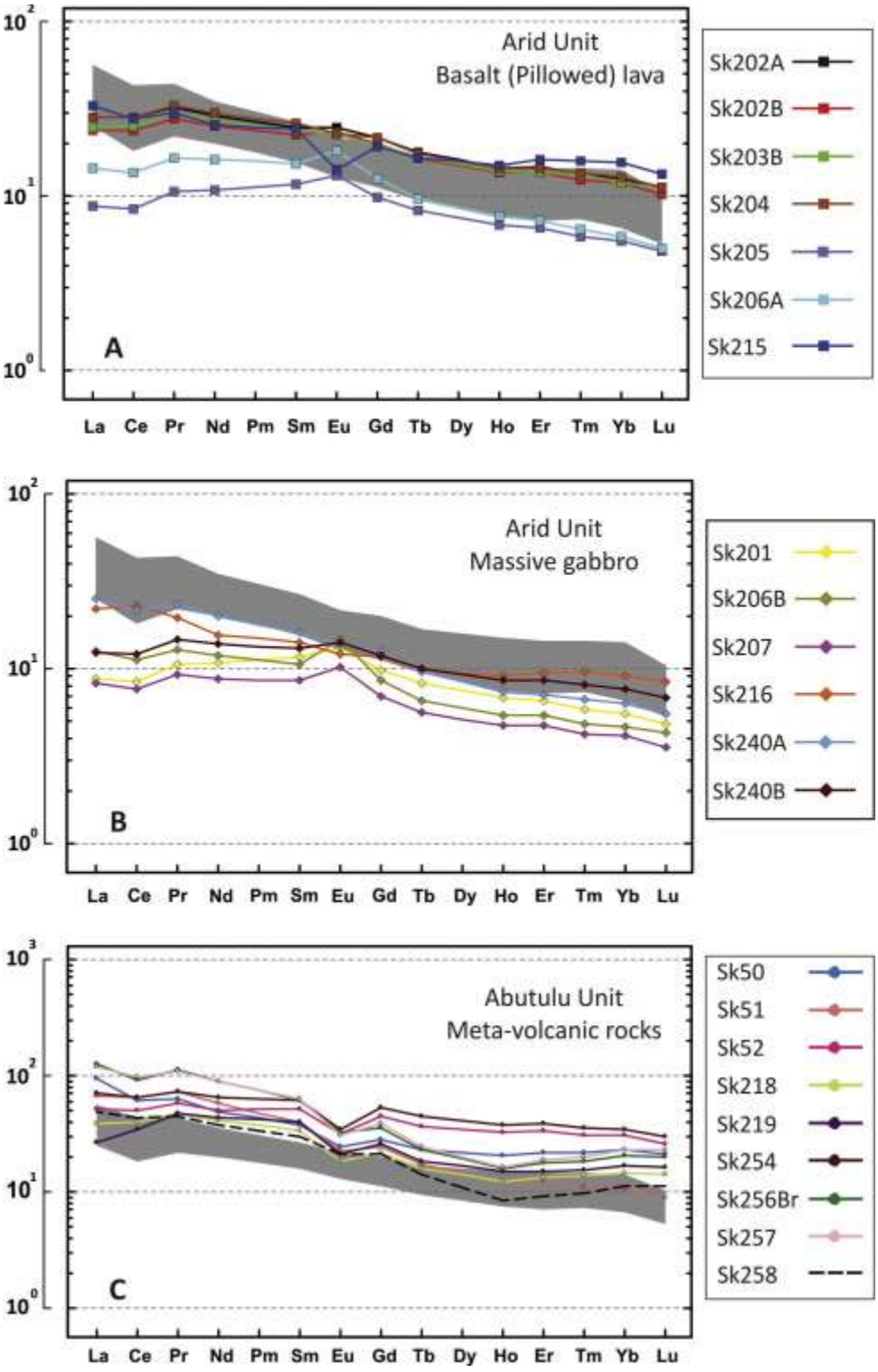

Fig. 8. Chondrite-normalized rare earth elements diagram for (a) pillow basalts, (b) massive gabbros and (c) the meta-andesite. Normalized values are from Sun and McDonough (1989). The grey shaded area represent samples Vanuatu arc.

of the subducting slab (Pearce et al., 1995; Tollstrup and Gill, 2005; Peate et al., 1997) and also to slab dehydration.

The chondrite normalized rare earth element diagram shows a fractionated pattern with high REE abundances (Fig. 8a). Eu anomaly is absent in most of the samples with the exception of Sk205 and Sk206A where both samples shows slight positive Eu anomaly (1.2 and 1.3 respectively) and sample Sk215 which shows a negative Eu anomaly of 0.7. The enrichment of the LREE relative to the HREE that is shown by all samples is a characteristic feature of arc lavas as well as back-arc lavas, (Peace & Stern, 2006) and correlates well with the Vanuatu arc (Peate et al., 1997) as shown on Fig. 8a.

In conclusion, we interpret the pillow basalt of the Abutulu area to represent basaltic volcanism of subduction-related arc/back-arc origin.

6.2. Massive gabbro

The massive gabbro from the Arid unit (Table 1) shows a wide range of SiO_2 from 44.81% to 58.45%, and also a wide range of TiO_2% from 0.25% (lower values usually found in basalts from a convergent tectonic setting) to 2.73% (values characteristic of basalts from extensional tectonic setting), but mostly < 1%, high MgO from 4.91% to 10.64% (with one sample showing low value of 2.14%), and low Fe_2O_3t from 5.44% to 13.22%. They also have a wide range of Al_2O_3 content from 13.94% - 19.58% and only three samples show high Al_2O_3 values (Table 1). The average Al_2O_3 content (17.62%) is close to the average of those reported for IAT and MORB but the anomalous samples fall within the average of high alumina basalt HAB (Brophy and March, 1985).

The Mg # shows higher values (32.7 to 68.56) than those of pillow basalt. Overall the Mg# exibits a gradational pattern that decreases from massive gabbros to the more basaltic andesite pillowed lava, suggesting increasing differentiation from a primary mantle derived magma with Mg# > 62 to more differentiated magma (cf., Luhr, 1997; Kampunzu et al., 1998).

The massive gabbro shows higher concentrations of Cr (251.4 ppm – 934.76 ppm) and Ni (25.7 ppm – 186.22 ppm), respectively (with few samples out of this range), than those of the pillow basalt and have element ratios comparable to those of the pillow basalts and hence of arc lavas (Table 1).

The massive gabbro MORB multi-element spiderdiagram of major and trace elements pattern shows a slight LREE enrichment and HFSE depletion, which is characteristic of mafic arc magmas (fig. 7b) and similar to that of Vanuatu arc (Peate et al., 1997). The moderate to slight LILE enrichments suggest a moderately evolved arc or back-arc environments (Küster and Liėgeois s, 2001). The only differences between the Vanuatu arc and the gabbros are the weaker negative Ta and Nb trough and the presence of negative Zr and Hf anomalies that are shown by sample SK206B and indicate the involvement of sediment components of the subduction slab, mantle-liquid interaction reaction or slab dehydration, a feature commonly seen in arc lava. Two of the massive gabbro samples (SK201 and SK207) show a relatively flat REE and strongly fractionated HREE $(Gd/Yb)_N$ between 1.7 to 2.0, possibly suggesting their generation through melting of an Fe-rich mantle corresponding to the stability fields of spinel and garnet peridotite at depths of 60-100 Km (Manikyamba et al., 2015).

The chondrite normalized rare earth elements pattern for the massive gabbro (fig. 8b) shows a LREE enrichment (La/Yb_N = 4.8, Sk209 excluded) and HFSE depletion characteristic of mafic arc magmas. The slight to moderate LILE enrichment indicates a primitive arc or back-arc

environment. A significant Eu anomaly (Eu/Eu* ≈ 1.2) dominates the massive gabbro with the exception of Sk 216 and Sk 240 (A & B) (Fig. 8b) indicating the role of accumulation of plagioclase in the genesis of the lower section of Arid unit (Rollinson, 1993; Preccerillo and Taylor, 1976). The three above mentioned samples that show no Eu anomaly also have a higher REE abundances ΣREE = (39.7 exclude 209).

To conclude, we interpret these gabbros to represent a lower section of the subduction related arc or back-arc magmas.

6.3. Basaltic andesites and andesite metavolcanic rocks

In the Zr/TiO_2 versus Nb/Y classification diagram (Fig. 6a) the metavolcanic rocks of the Abutulu unit are classified as basaltic andesite and andesite with most of the samples falling in the latter category.

The metavolcanic rocks are characterized by moderate silica (42.8% – 64.87%) and relatively high TiO_2 (up to 2.40%), Al_2O_3 (11.96% - 17.59%), Fe_2O_3t (5.12% - 15.71%) and MgO (2.13% - 9.75%). Transitional metals (Cr & Ni) reach an average of 135.49 ppm and 22.36 ppm, respectively (Table 2).

On MORB-normalized multi-element incompatible element plot (Fig. 7c), the meta-andesite shows LILE-enriched, HFSE depleted patterns characteristic of arc derived magma, a well developed negative Nb-Ta trough (with variable degree of depletion) and a negative Zr-Hf trough that is shown by sample SK51. All of these are features of subduction-related magmas. The meta-andesite shows a better correlation with the Vanuatu arc than the massive gabbro and the pillowed basalt. The main difference between the meta-andesite and the massive gabbro and basalt is the enrichment of Th in the meta-andesite relative to MORB, which may indicate an

increasing sedimentary component from the subducting slab (Plank, 2005) or an increase in the thickness of the arc crust which allows Th enrichment (Kuster and Liégeois, 2001 and reference therein).

The chondrite-normalised REE diagram of the Abutulu metavolcanic (meta-andesite) rocks (Fig. 8c) shows a fractionated pattern similar to those of the Arid unit (lava and gabbro), however the REE abundances is higher than those of the basalts and the gabbro ($\Sigma REE \approx 156.7$). A negative Eu anomaly ($Eu/Eu^* = 0.67$) is a pronounced feature in the REE pattern of all Abutulu metavolcanic data. The metavolcanic rocks are enriched in LREE and show good correlation in the REE pattern with the Vanuatu arc (Peate et al., 1997).

To conclude, we interpret the Abutulu meta-andesite as erupted from evolved subduction related arc or back-arc magma.

7. Geochronology and isotope geochemistry

Twelve samples representing the metavolcanic rocks of the Arid and Abutulu units were selected for analysis of their Rb-Sr and Sm-Nd isotope compositions (Table 3). The Geodate software (Eglington and Harmer, 1999), which uses algorithms similar to those of Lugwig (1999), was used for the calculation of ages. Geodate software only accepts the errors given at 1σ level.

Nd- and Sr-isotope analyses were conducted at the Department of Geological Science, University of Cape Town, South Africa. Sample powders were dissolved using Hf-HNO_3 acid mixture in closed Teflon beakers on hotplates at 140°C for 2 days. Any minor undissolved material was removed by centrifuging the samples prior to sequential Sr and Nd separation chemistry (Pin et al., 1994; Míková & Denková, 2007; Pin & Zalduegui, 1997). Final Sr and Nd

Table 3. Isotopic data of the low-grade Arid and Abutulu units from the western Nuba Mountains. T_{DM} Nd model ages were calculated after Nelson and DePaolo (1985) for rocks with $^{147}Sm/^{144}Nd < 0.165$.

Rb		Sr	$^{87}Rb/^{86}Sr$	$^{87}Sr/^{86}Sr$	2σ	Sri at 778 Ma	Sm	Nd	$^{147}Sm/^{144}Nd$	$^{143}Nd/^{144}Nd$	2σ	Ndi at 778 Ma	Nd at 778 ± 90 Ma	TDM Ma
sk-202a	1.76	624	0.0081	0.703628	0.000013	0.703537	4.48	17.3	0.1566	0.512757	0.000009	0.511919	+6.4±0.5	778
sk202b	2.68	711	0.0109	0.703693	0.000016	0.703572	4.05	15.1	0.1625	0.512779	0.000009	0.511908	+6.2±0.4	802
sk-203b	3.02	748	0.0117	0.704188	0.000012	0.704058	4.31	16.1	0.1618	0.512767	0.000009	0.511900	+6.1±0.4	825
sk-204	2.99	901	0.0096	0.704036	0.000015	0.703930	4.69	17.9	0.1586	0.512757	0.000009	0.511907	+6.2±0.5	807
sk-240	10.5	316	0.0959	0.703415	0.000015	0.702349	2.38	8.26	0.1744	0.512813	0.000007	0.511879	+5.7±0.3	905
sk-240a	1.98	286	0.0201	0.703020	0.000012	0.702797	2.93	11.9	0.1487	0.512663	0.000008	0.511867	+5.3±0.6	899
sk-254	2.28	74.0	0.0892	0.704266	0.000010	0.703275	11.1	39.0	0.1303	0.512798	0.000007	0.511876	+5.7±0.3	859
sk255	36.5	51.0	2.0751	0.721407	0.000012	0.698354	4.23	19.6	0.1242	0.512577	0.000006	0.511880	+5.5±0.8	792
sk256	84.2	41.4	5.9156	0.753392	0.000011	0.687676	11.1	53.9	0.1291	0.512584	0.000008	0.511918	+6.2±0.8	789
sk257	0.56	59.2	0.0274	0.704842	0.000010	0.704537	11.4	53.2	0.1478	0.512611	0.000007	0.511919	+6.3±0.8	854
sk258	14.1	157	0.2605	0.706625	0.000010	0.703732	5.47	22.4	0.1566	0.512678	0.000007	0.511886	+5.7±0.6	778
sk-014	4.15	197	0.0609	0.704823	0.000015	0.704146	4.47	17.2	0.1567	0.512776	0.000006	0.511937	+6.8±0.5	732

fractions were analysed for isotopic compositions using a Nu Instruments DSN-100 desolvating nebuliser and NuPlasma HR-MC-ICP-MS instruments.

The external 2 sigma errors for the measured Sr and Nd isotope ratios are better than ± 0.000015. The BHVO-2 basaltic standard reference material yields values of 0.703530±0.000009 for 86Sr/88Sr and 0.513005±0.000009 for $^{134}Nd/^{144}Nd$, comparing well with published data (Weis et al., 2006).

Concentrations of Rb, Sr, Sm and Nd were measured using ICP-MS. The error on Rb/Sr and Sm/Nd is <4%.

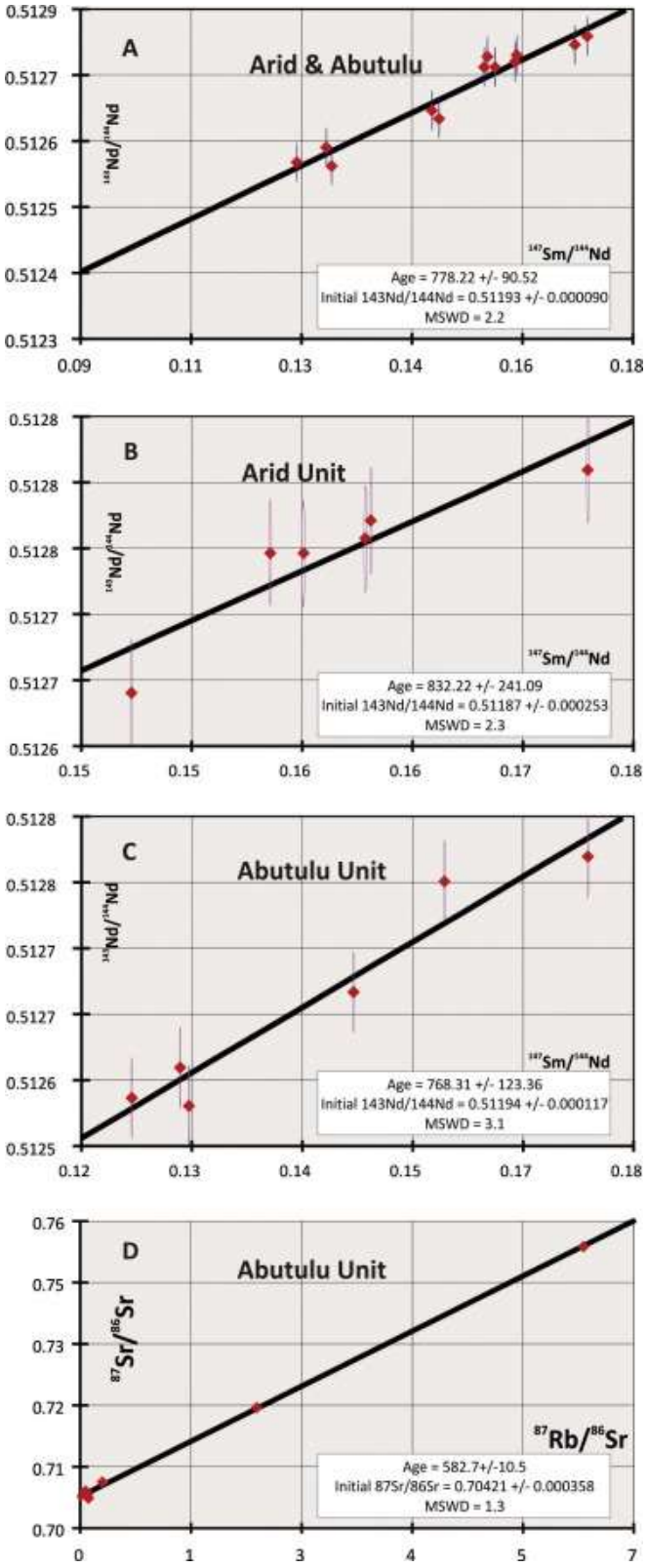

Fig. 9. (A) Sm–Nd robust regression plotting for 12 metavolcanic samples of Arid and Abutulu units (B) Sm–Nd isochron for 6 meta-basalts of Arid unit (C) 6 point Sm–Nd errochron for the meta-andesite of Abutulu unit (D) Rb–Sr isochron for 6 metavolcanic samples of the Abutulu unit.

7.1. Sm-Nd whole rock dating and Nd initial isotopic ratios

The regression of 12 samples gave an isochron of 778 ± 90 Ma, Nd initial ratio ($NdIR_{778}$) = 0.51193±0.000090 equivalent to $\varepsilon_{Nd778\pm90}$ = +5.9 ± 1.8, MSWD = 2.2 (Fig. 9a). When each group of the metavolcanic rocks are plotted separately, Arid unit produced a 6 point WR isochron of 835 ± 241 Ma, $NdIR_{835}$ = 0.51187 ± 0.000253 ($\varepsilon_{Nd835\pm241}$ = +6.2 ± 4.9), MSWD = 2.3 (Fig. 9b), while the Abutulu unit produced a 768 ± 123 Ma, $NdIR_{768}$ = 0.51194±0.000117, ($\varepsilon_{Nd768\pm123}$ = +5.8 ± 2.3), MSWD = 3.1 for 6 WR errorchron (Fig. 9c).

The ε_{Nd} of the samples shows no direct correlation with SiO_2 and hence the low values of ε_{Nd} are not linked to AFC processes.

7.2. T_{DM} Nd model ages

The Sm/Nd ratios of the mafic and ultra-mafic rocks are close to the mantle ratios which preclude the calculations of meaningful T_{DM} Nd model ages, for this reason only samples with Sm^{147}/Nd^{144} < 0.165 were selected for calculation of Nd model age (Table 3; calculated following Nelson and De Paolo, 1985).

The average values of T_{DM} Nd model age of 10 samples that pass the Sm^{147}/Nd^{144} < 0.165 filter is 814 Ma. This age is very close to the emplacement age. T_{DM} Nd model ages that are so close to the emplacement age indicates no contribution from older crustal material in the genesis of the metavolcanic rocks of the western Nuba Mountains.

7.3. Rb – Sr whole rock dating

Low Rb/Sr ratios of the Arid pillow basalt prohibited the calculation of a meaningful age. The meta-andesite and basaltic andesite of Abutulu provide a 6 point isochron (MSWD = 1.3) of 582 ± 10 Ma (Fig. 9d) equivalent to SrIR = 0.70421 ± 0.000358.

The low radiogenic growth of the metavolcanic rocks as a result of their low Rb/Sr ratios allows for the calculation of an accurate initial ratio (Kuster and Liegeois, 2001) at 778 Ma (with the exception of two acidic samples from Abutulu unit). The average initial ratio of the metavolcanic rocks is 0.703593 for 10 whole rock samples, consistent with ε_{Nd}+5.9 and in agreement with a juvenile mantle source.

The samples with low initial $^{87}Sr/^{86}Sr$ ratios (Sk 255; 0.699158 and Sk 256; 0.689969) have values corresponding to ε_{Nd778} of +5.4 and +6.1, respectively, and T_{DM} Nd model ages similar to the rest of the metavolcanic rocks.

8. Discussion

8.1. Lithology and structure of the metavolcanic rocks

Geological mapping of the area between Lagawa in the east, Abutulu in the west, Abu Zabad in the north and Gingaro in the south reveals the southwestward continuation of the NE-trending belt of low-grade metavolcanic and metasedimentary rocks (Sadig and Vail, 1986) from Abu Zabad through the known occurrences of Abutulu and further to the southwest (Fig. 2 and 3 (A and B)). The nature of the outcrops within the belt are generally scattered and found as isolated hills of low-lying topographic relief. Outcrops are of basic to intermediate metavolcanic rocks, slate, phyllite, graphitic and mica quartzitic schist. They are intensively sheared and folded in a pattern typical of sinistral transpression tectonics. Mafic complexes are found only along the

eastern flank of the metavolcanic rocks. The nature of the latter complexes is similar to that of oceanic crust with a cumulate section composed mainly of layered gabbro and minor hornblendite and an upper section mainly of massive gabbro and basaltic pillowed lavas. The presence of several gabbroic plutons beneath the extrusive metavolcanic rocks, seen in the field and interpreted from geophysical data (Sadig and Vail, 1986, Vail, 1973; this work), is consistent with this interpretation. The sheeted dolerite dykes and the basal section typical of preserved ancient ocean crust have not been observed except for talc-carbonate rocks found at the southern part of Al Beida, which might be interpreted as altered serpentinite ultramafic rock, and thus part of the typical basal sequence. Conventionally, the existence of sheeted dolerite dykes in ophiolite is considered as strong evidence for the origin of oceanic crust now exposed on land, by sea floor spreading (Gass, 1990; Moores and Vine, 1971) This idea is now debated (Dilek and Furnes, 2011) since the formation of a sheeted dyke complex requires a delicate balance between the spreading rate and the magma injection rate, which is difficult to maintain in a supra-crustal tectonic environment (Robinson et al., 2008). The lack of sheeted dykes may indicate a spreading rate lower than the rate of magma production in the region (Robinson et al., 2008; Dilek and Furnes, 2011). The rock association and structure of the mafic and ultramafic rocks show close similarities to those rock associations defined as ophiolitic by the Penrose conference (Anon, 1972; Coleman, 1977). Also, the lack of any thermal impact of these complexes on the surrounding gneiss and the absence of any mafic off-shoots and apophyses along the surrounding bounding lithologies support their ophiolitic origin.

Petrographic studies of both the metavolcano-sedimentary sequence and the mafic and ultramafic complexes show mineral assemblages composed of epidote, chlorite, actinolite and albite, indicative of the greenschist facies of regional metamorphism. A high-pressure metamorphic

event is suggested by the presence of glaucophane within the mineral assemblage of the metasedimentary rocks (Mansour and Iskander, 1960). However glaucophane has never been seen in the samples examined in this study. This metamorphic rock association is in sharp contrast to the higher-grade (upper amphibolite facies) granitic and granodioritic gneiss to the east. The steeply southeasterly dipping shear zone is considered to mark the boundary between the two units.

8.2. The geodynamic context

The Neoproterozoic arc/back-arc metavolcano-sedimentary sequence of the westernmost Nuba Mountains (≈ 300 Km west of Kabus suture) are bounded by high-grade gneiss in both the eastern and western sides. The high-grade gneiss of western Sudan generally reflects Early to Middle Proterozoic crust formation ages with evidence of significant remobilization of older crust (Vail, 1990 and references therein). Sm-Nd T_{DM} model age data from the Wadi Howar (1300 Ma, ε_{Nd} = -6.7; Schandelmeier et al., 1988), from the Nubian Desert (>2200 Ma, ε_{Nd} = -15.8, 1137 Ma, ε_{Nd} = -6.5; Schandelmeier et al., 1988) and from as close to the study area as El Obeid in North Kordofan (>2000 Ma, εNd = -10.3; Harris et al., 1984) support this suggestion. Younger K-Ar and Rb-Sr ages were obtained from all of the previously mentioned areas and interpreted to represent a Pan-African imprint (see Vail, (1990) for full compilation of the geochronological data and for the context in which the term “Pan-African imprint” is used). The younger Rb-Sr age (relative to Sm-Nd age) obtained in this study is also interpreted to represent disturbance of Rb/Sr system by the late Pan African metamorphism. The metamorphism and/or alteration that affect all of the lithologies described in section 3 provide evidence to support open system behavior for the Rb/Sr system. Because of the absence of any previous geochronological

work on the low-grade rocks of the Nuba Mountains region it is not clear whether this mobility of the Rb/Sr system is due to younger HT metamorphism or to final uplift and crustal cooling in the region as suggested for the basement rocks of the Sabaloka area immediately west of the eastern boundary of the SMC in north central Sudan, at around 622 Ma (Kuster and Liėgeois, 2001 and reference therein). The limited Nd model age data available on the eastern Precambrian outcrops only suggest an early Neoproterozoic age (Harris et al., 1984) for the crust with ε_{Nd750} between +2.2 and +3.5 for the Rashad and Abbasiya outcrops (immediately west of Kabus suture) and are interpreted as suggesting the presence of oceanic material in the crust of central Sudan (Harris et al., 1984).

The model of Abdelsalam and Dawoud (1991) assumes two successive stages of easterly dipping subduction for the development of the northeastern Nuba Mountains metavolcanic rocks and the associated ophiolite. The first resulted in the formation of an intra-oceanic arc (now the metavolcanic sequence of the northeastern Nuba Mountains) and a marginal basin to the west of the arc (now Kabus ophiolite and the metasedimentary rocks of NE Nuba Mountains), the second subduction of the newly formed oceanic crust has led to the formation of the Kabus ophiolitic mélange, as well as an Andean-type arc further west. According to this model pre-Pan-African crust exists underneath the now eroded Andean-type arc and is separated from the ANS by the Kabus suture.

Unfortunately, there are no isotopic data available on the Pan-African low-grade metavolcanic rocks east of the Kabus suture to assist in correlating the mantle source in the eastern and western Nuba Mountains. However, if we consider the mantle source of the ANS as one entity (although there are some differences in the ε_{Nd} values across the shield), the isotopic composition of the mantle source of the western Nuba Mountains (average limit ε_{Nd} for 12 metavolcanic rocks

≈ +6 at 778 Ma) is similar to the mantle source reported for the ANS (when considering the errors and uncertainty associated with Sm-Nd data) that is from +6.5 to +8.4 (Stern and Abdelsalam, 1998). According to the model of Abdelsalam and Dawoud (1991), assuming an Andean-type arc west of the Kabus suture, one would expect the geochronological data obtained from the medium-grade gneiss and the granitoid intrusions that intrude the gneiss unit to reflect an isotopic signature that shows contamination with underlying older rocks. The data obtained by Harris et al., (1984) on the syn-tectonic granite of Rashad and Abbassyia (T_{DM} 1000 and 950 Ma and $\varepsilon_{778\ Nd}$ of +2.5 and +3.7) are in good agreement with the Nd model ages obtained during the course of the current study on three granitic and granodioritic gneisses in the vicinity of Jebel Lagawa (data are not presented, see Fig 3 for location of Jebel Lagawa). These indicate $\varepsilon_{778\ Nd}$ value of +4.3 and a T_{DM} Nd model age of around 937 Ma for crustal formation.

With the exception of the higher initial Sr ratio (0.7060) at 514 ± 17Ma of the Jebel Doleibayia outcrop, which is interpreted as the assimilation of older crust (Curtis and Lenz, 1985), all of the initial Sr ratios obtained by the same authors from the anorogenic granite of Ed Dair and Liri as well as the initial Sr ratio obtained by Harris et al., (1984) on the Syenite of Dumbier suggest either a less depleted mantle source or formation from juvenile crust. Although the number of data is not large enough to systematically cover the large gneiss unit between the Kabus suture and the Abutulu shear zone, the wide area covered by the samples, the various lithologies of the samples and the tight cluster of the data in both the T_{DM} Nd model ages and the ε_{Nd} would exclude the possibility of even a small contribution of older crust. Based on this assumption we consider the possibility of having older crust between Kabus and Abutulu as highly unlikely, and hence we suggest that the Andean-type arc suggested by Abdelsalam and Dawoud (1991) should be considered instead as intra-oceanic arc.

There is no geochronological data to date the initiation of the subduction that formed the proposed intra-oceanic arc. However, Küster et al., (2008) identified the age of the early Pan-African accretionary phase in the ANS to be between 850 and 650 Ma. The age of the oceanic lithologies in the ANS was found to be between 890 and 690 Ma (Stern et al., 2004).

8.3. Proposed tectonic model

The co-existence and occasional intercalation between Neoproterozoic arc/back-arc metavolcanic rocks, arc related sedimentary rocks and turbiditie necessitate the existence of an early Neoproterozoic marginal basin (i.e. before 778 Ma the age of metavolcanic rocks) further west of the intra-oceanic arc. The arc/back-arc signature of the metavolcanic rocks precludes the simple model assuming opening and closing of a small marginal basin without developing subduction zones as has been proposed for the Rahib fold and thrust belt in northwestern Sudan (Abdelrahman et. al., 1990). Whether this marginal basin is formed due to the subduction zone that formed the intra-oceanic arc or to the other east-dipping subduction zone possibly to the west of Abutulu (since the vergence of the major structure is uniformly to the west) is beyond the scope of this paper. However, for simplicity we will adopt the west-dipping subduction of Abdelsalam and Dawoud, (1991) (Fig. 10a). The error on the ages does not allow for accurate estimation of the period of arc activity. At a later stage (after the 778 Ma age of arc magmatism) the basin started receiving sediments from the western continental side and possibly from the eastern intra-oceanic arc. This stage also witnessed the emplacement of the arc-related gabbroic intrusions (Fig. 10b).

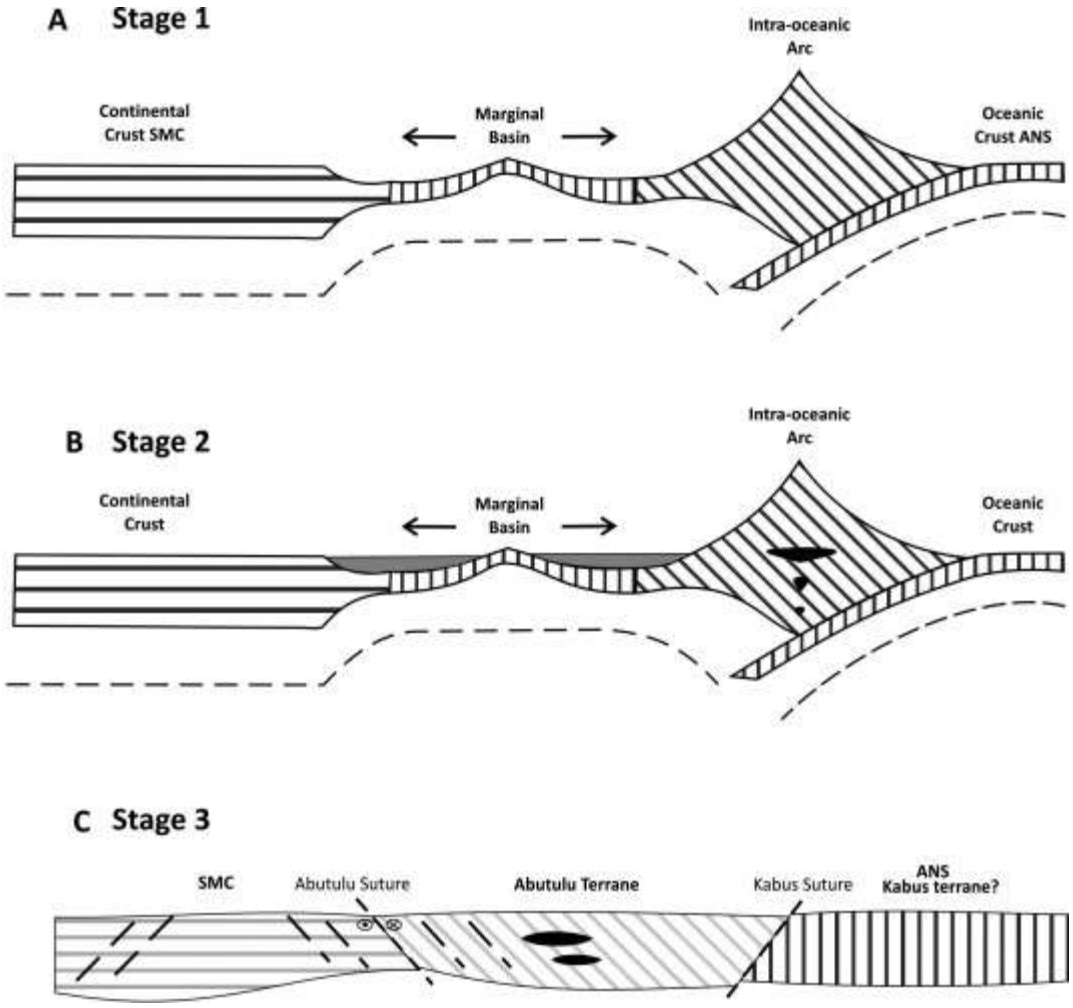

Fig. 10. Proposed tectonic model to explain the evolution of the western Nuba Mountains. (a) Development of intra-oceanic arc over a westerly-dipping subduction zone and later development of small marginal basin to the west of the intra-oceanic arc. (b) The marginal basin starts receiving sediments from both the arc side and the continental side and the emplacement of gabbroic sills and intrusions within the arc. (c) Closing of the marginal basin and the development of Abutulu sinistral shear zone.

The closure of the basin took place sometime after the accumulation of the continental sediments and the continental block to the west collided against the arc/back-arc assemblage which led to the development of the Abutulu sinistral shear zone (Fig. 10c).

Future dating of Hagar El Tair and Um Shair syntectonic granite intrusions and granodiorite affected by the sinistral shearing may set good constraints on the lower age of this collision.

Post-collisional tectonism took place probably until around 550 Ma (the age of the alkaline granitoids of Ed Dumbier and Ed Dair) (Harris et.al., 1984).

We further suggest that the Neoproterozoic Pan-African crust indeed exists further west of the Kabus suture (at least as far as the Abutulu metavolcanic unit). Also, the Abutulu shear zone may represent a major geological suture separating not only rocks of different lithology, grade of metamorphism and structural style but it also separates terrenes of different age and mantle sources. The Neoproterozoic crust of the western Nuba Mountains can be correlated with that of the Bayuda desert in north central Sudan in terms of age (806 Ma for the Bayuda and 778 Ma for the Nuba Mountains), geochemical affinity (both show an arc-related signature) and structural trends (both show a NE-trend of foliation) and may then support Küster and Liégeois' (2001) proposed hypothesis that the boundary of the SMC (referred to as the East Saharan ghost craton) must lie below or further west than what was previously expected.

9. Conclusions

- Geological mapping of the area between Abu Zabad and Abutulu, southern Sudan, confirms that a low-grade metavolcano-sedimentary sequence (meta-andesite, meta-basalt, slate, graphitic and quartzitic schist) are continuous throughout the area. This sequence is associated with occurrences of mafic and minor ultramafic rocks that show most of the features typical of Penrose conference-type ophiolite structures.
- The mafic complexes have all of the geochemical characteristics set by Dilek and Furnes (2011) for back-arc supra-subduction ophiolites and hence they are considered to

represent remnants of a continental back-arc basin that developed to the west of the Kabus ophiolitic melange.

- On the basis of the variation in lithology, geochemistry, inferred tectonic environment and isotopic characteristics, the low-grade metavolcano-sedimentary sequence and associated supra-crustal back-arc ophiolite are considered to represent a Neoproterozoic arc terrane, the 'Abutulu terrane', that extends from Abu Zabad in the north to a few kilometers southwest of Abutulu in the south. These rocks are separated from the Early Neoproterozoic continental lithologies in the east by the Abutulu sinistral shear zone. Its western boundary against the pre-Neoproterozoic SMC is hidden under the Quaternary sediments of the Nuba Mountains.
- It is possible that the Abutulu Shear Zone represents the eastern edge of the SMC, approximately 300km further west than was previously thought (Abdelsalam and Dawoud, 1991).

10. Acknowledgments

The authors are grateful to the staff of the Faculty of Petroleum and Minerals of Al Neelain University, Sudan, especially Dr Salih for field work assistance, and to Dr Sami for providing Landsat data. Our thanks are also due to the National Research Foundation (NRF) South Africa, University of Al Neelain and the Geological Research Authority Sudan for their financial and logistical support. We acknowledge the input of Jean-Paul Liégeois and an anonymous reviewer, and associate editor Natasha Wodika who greatly improved on an earlier version of this work.

References

Abdel-Rahman, E.M., Harms, U., Schandelmeier, H., Franz, G., Darbyshire, D.P.F., Horn, P., Muller-Sohnius, D., 1990. A new ophiolite occurrence in NW Sudan—Constraints on late Proterozoic tectonism. Terra Nova. Vol. 2, 363–376.

Abdelsalam, M.G., Dawoud, A.S., 1991. The Kabus ophiolitic melange, Sudan, and its bearing on the W boundary of the Nubian Shield. Journal Geological Society, London. Vol. 148, 83–92.

Abdelsalam, M., Liégeois, J.P., Stern, R.J., 2002. The Saharan metacraton. Journal of African Earth Sciences. Vol. 34, 119–136.

Anon, 1972. Penrose Conference on ophiolites. Geotimes 17, 24–25.

Brinkmann, K., 1982. Mineral prospecting in the northeast Nuba Mountains, southern Kordofan. Federal Institute for Geosciences and Natural Resources (BGR) Report, West Germany, Hannover.

Brinkmann, K.,1986. Geology and mineralization of the basement complex in the northeastern Nuba Mountains, Sudan. Geologisches Jahrbuch.Vol. 64**,** 3-34.

Brophy and March, 1985. On the Origin of High-Alumina Arc Basalt and the Mechanics of Melt Extraction. Journal of Petrology. Vol. 27, Part 4. 763-789.

Browne, S**.** E. and Fairhead, S**.** D. 1983. Gravity study of the Central African Rift System: A model for continental disruption, 1. The Ngaoundere and Abu Gabra Rifts. Tectonophysics. Vol. 94, 187-203.

Cann, J. R., 1970. Rb, Sr, Y, Zr and Nb in some ocean floor basaltic rocks. Earth and Planetary Science Letters. Vol. 10, 7 - 11.

Coleman, R.G., 1977. Ophiolites. Springer-Verlag, Berlin, 229 pp.

Curtis, P. and Brinkmann, K., 1985. The geology of younger intrusive alkali complexes in the southwestern Nuba Mountains, Sudan. Geologisches Jahrbuch. Vol. B63, 3-4, Hannover.

Denkler, T., Franz, G., Schandelmeier, H., 1994. Tectonometamorphic evolution of the Neoproterozoic Delgo suture zone, northern Sudan. Geologische Rundschau. Vol. 83, 578 - 590.

Dilek, Y. and Furnes, H., 2011. Ophiolite genesis and global tectonics: Geochemical and Tectonic fingerprinting of ancient oceanic lithosphere. Geological Society of America Bulletin. Vol. 123, 387- 411

El Ageed, A. I. and El Rabaa, S**.** M. 1980. The geology and structural evolution of the northeart Nuba Mounrains, Southern Kordofan Province, Sudan. Bulletin of the Geological and Mineral Resources Authority of the Sudan, No. 32.

El Ageed, A. I. 1974. The geology and iron mineralization in the northeast Nuba Mountains, Kordofan Province, Sudan**.** MSc thesis, University of Khartoum**.**

El Nadi, A. I. 1980. The geology of the Keig El Kheil, Damik and Umm Dugo igneous complexes, Nuba Mountians, Sudan. M. Sc. thesis. Univ. Khartoum (unpublished).

Gass, I.G., 1990, Ophiolites and oceanic lithosphere, *in* Malpas , J., Moores, E.M., Panayiotou, A, and Xenophontos, C., eds., Ophiolites, Oceanic Crustal Analogues, Proceedings of the Symposium “Troodos 1987”: Nicosia, Cyprus, The Geological Survey Department. 1–10.

Harms, U., Darbyshire, D.P.F., Denkler, T., Hengst, M., Schandelmeier, H., 1994. Evolution of the Neoproterozoic Delgo sutures zone and crustal growth in northern Sudan: geochemical and radiogenic isotope constrains. Geologische Rundschau. Vol. 83, 591– 603.

Harms, U., Schandelmeier, H., Darbyshire, D.P.F., 1990. Pan-African reworked early/middle Proterozoic crust in NE Africa W of the Nile: Sr and Nd isotope evidence. Journal Geological Society, London. Vol. 147, 859–872.

Hart, R., 1970. K, Rb, Cs contents and K/Rb, K/Cs ratios of fresh and altered submarine basalts. Earth Planet. Sci. Lett. Vol. 6, 295–303.

Harris, N.B.W., Hawkesworth, C.J., Ries, A.C., 1984. Crustal evolution in north-east Sudan and East Africa from model Nd ages. Nature. Vol. 309, 773–776.

Hashiguchi, H., Yamada, R., and Inoue, T., 1983. Practical application of low Na2O anomalies in footwall acid lava for delimiting promising areas around the Kosaka and Fukazawa Kuroko deposits, Akita Prefecture, Japan. In: Ohmoto, H., et al., (eds.). The Kuroko massive sulfide deposite. Economic geology Monograph. Vol. 5, 387 - 394.

Hastie, A.R., Kerr, A.C., Pearce, J.A. and Mitchelle, S.F., 2007. Classification of altered volcanic island arc rocks using immobile trace elements: Development of the Th - Co discrimination diagram. Journal of Petrology. Vol. 48 no.12, 2341- 2357.

Hirdes, W. and Brinkmann, K**.**, 1985. The Kabus and Balula serpentinite and metagabbro complexes: A dismembered ophiolite in northeastern Nuba Mountains, Sudan. Geologisches Jahrbuch. Vol. 58**,** 3 - 43.

Hill, I. G., Worden, R. H. and Meighan, I. G., 2000. Yttrium: The immobility – mobility transition duing basaltic weathering. Geology Vol. 28, 923 – 926.

Hynes, A., 1980. Carbonitization and mobility of Ti, Y and Zr in Ascot formation metabasalt, S.E. Quebec. Contributions to Mineralogy and Petrology. Vol. 75, 79 – 87.

Humphris, S.E., and Thompson, G., 1978. Hydrothermal alteration of oceanic basalts by seawater. Geochimica et Cosmochimica Acta. Vol. 42, 107–125.

Kampunzu, A.B., Bonhomme, M.G., and Kanika, M., 1998. Geochronology of volcanic rocks and evolution of the Cenozoic Western branch of the East African rift system. Journal of African Earth Sciences. Vol. 26, 441–461.

Kröner, A. and Stern, R. J., 2004. Pan-African Orogeny. Encyclopedia of Geology, Vol. 1, Elsevier, Amsterdam.

Küster, D. and Liegeois, J. P., 2001. Sr, Nd isotopes and geochemistry of the Bayuda Desert high-grade metamorphic basement (Sudan): an early Pan-African oceanic convergent margin, not the edge of the East Saharan ghost craton? Precambrian Research. Vl. 109, 1-23.

Küster, D., Liégeois, J.P., Matukov, D., Sergeev, S., Lucassen, F., 2008. Zircon geochronology and Sr, Nd, Pb isotope geochemistry of granitoids from Bayuda Desert and Sabaloka (Sudan): evidence for a Bayudian event (920–900 Ma) preceding the Pan-African orogenic cycle (860–590 Ma) at the eastern boundary of the Saharan Metacrat. Precambrian Research. Vol. 164, 16–39.

Liégeois, J. P., Abdelsalam, M. G., Ennih, N, and Ouabadi, A., 2013. Metacraton: Nature, genesis and behavior, Gondwana Research. Vol. 23 (2013), 220–237

Ludwig, K.R., 1999. Using Isoplot/Ex Version 2.01, A Geochronological Toolkit for Microsoft Excel. Berkeley Geochronology Center Special Publication No. 1a, Berkeley, CA, 47 pp.

Luhr, J. F., 1997. Extensional tectonics and diverse primitive volcanic in the western Mexican volcanic belts. Canadian Mineralogist. Vol. 35, 473 - 500.

Lyns, H. and Campbell-Smith, W., 1921. Preliminary note on rocks of Darfur. Geol. Mag. Vol. 58, 206 - 215.

Mansour, A. O. and Samuel, A., 1957. Geology and hydrogeology of sheet 66-A Rashad and sheet 66-E Talodi. Geological Survey, Sudan. Mem. 1.

Mansour, A. O. and Iskander, W., 1960. An Iron ore deposit at Jebel Abutulu. Geological Survey, Sudan. Bull. 6.

Manikyamba, C., Sohini Ganguly, M., Santosh, M., Abhishek Saha and Lakshminarayana. G., 2015. Geochemistry and petrogenesis of Rajahmundry trap basalts of Krishna-Godavari Basin, India. Geoscience Frontiers. Vol. 6(2015), 437 – 451.

McCulloch, M. T., & Gamble, J. A., 1991. Geochemical and geodynamical constraints on subduction zone magmatism. Earth and Planetary Science Letters. Vol. 102, 358 – 374.

Míková J., Denková P., 2007. Modified chromatographic separation scheme for Sr and Nd isotope analysis in geological silicate samples. Journal of Geosciences. Vol. 52, 221–226. DOI: 10.3190/jgeosci.015

Moores, E.M., and Vine, F.J., 1971. The Troodos massif, Cyprus, and other ophiolites as oceanic crust: Evaluation and implications: Philosophical Transactions of the Royal Society of London, Vol. 268A, 443 – 466.

Mottl, M.J., 1983. Metabasalts, axial hot springs, and the structure of hydrothermal systems at mid-ocean ridges. Geo. Soc. Am. Bull., Vol. 94, 161-180.

Nelson, B.K., DePaolo, D.J., 1985. Rapid production of continental crust 1.7 to 1.9 b.y. ago: Nd isotopic evidence from the basement of the North Americam midcontinent. Geol. Soc. Am. Bull. Vol. 96, 746–754.

Pearce, J.A., 2008. Geochemical fingerprinting of oceanic basalts with applications to ophiolite classification and the search for Archean oceanic crust. Lithos. Vol. 100 14 – 48.

Pearce, J. A., and Cann, J. R., 1973. Tectonic setting of basic volcanic rocks determined using trace element analyses. Earth and Planetary Science Letters. Vol. 19, 290 - 300.

Pearce, J. A and Stern, R. J., 2006. Origin of Back-Arc Basin Magmas: Trace Element and Isotope Perspectives. Back-Arc Spreading Systems: Geological, Biological, Chemical and Physical Interactions. Geophysical Monograph Series 166 Published in 2006 by the American Geophysical Union 10.1029/166GM06

Pearce, J. A., Baker, P.E., Harvey, P.K., and Luff, I.W., 1995, Geochemical evidence for subduction fluxes, mantle melting and fractional crystallization beneath the south Sandwich island arc. Journal of Petrology. Vol. 36. 1073-1109.

Peate, D.W., Pearce, J.A., Hawkesworth, C.J., Colley, H., Edwards, C.M.H. and Hirose, K., 1997. Geochemical variations in Vanuatu arc lavas: the role of subducted material and a variable mantle wedge composition. Journal of Petrology. Vol. 38 no. 1331–1358.

Pin C., Zalduegui J.F.S., 1997. Sequential separation of light rare-earth elements, thorium and uranium by miniaturized extraction chromatography: application to isotopic analyses of silicate rocks. Anal Chim Acta, Vol. 339, 79 – 89

Pin C., Briot D., Bassin C., Poitrasson F., 1994. Concominant Separation of strontium and samarium–neodymium for isotopic analysis in silicate samples, based on specific extraction chromatography. Anal Chim Acta, Vol. 298, 209–217

Plank, T., 2005. Constraints from Thorium/Lanthanum on Sediment Recycling at Subduction Zones and the Evolution of the Continents. Journal of Petrology. Vol. 46 no. 921– 944.

Polat, A., Kerrich, R., Wyman, D., 1999. Geochemical diversity in oceanic komatiites and basalts from the late Archean Wawa greenstone belt, Superior Province, Canada: trace element and Nd isotope evidence for a heterogeneous mantle. Precam. Res. Vol. 94, 139–173.

Preccerillo A. and Taylor S. R., 1976. Geochemistry of Calc-Alkaline Volcanic Rocks from the Kastamonu Area, Turkey, Contribution to Mineralogy and Petrology, Vol. 58, 63-81.

Qureshi, I. R. and Sadig, A. A., 1967. Earthquakes and associated faulting in Central Sudan. Nature, Vol. 215, no. 5098, 26 – 35.

Robinson, P.T., Malpas, J., Dilek, Y., and Zhou, M.F., 2008. The significance of sheeted dike complexes in ophiolites: GSA Today, Vol. 18, no. 11, 4–10.

Rollinson, Hugh. R., 1993. Using Geochemical Data: Evaluation, Presentation, Interpretation. Longman Geochemistry Series, Harlow, England.

Shkol'nik S.I., Reznitskii, L.Z., Belichenko, V.G., Barash, I.G., 2009. Geochemistry, petrogenesis, and geodynamic typification of metavolcanics of the Tunka terrane (Baikal–Hövsgöl region). Russian Geology and Geophysics Vol. 50 (2009) 779–788.

Sadig, A, . A. and Vail, J**.** R., 1986. Geology and regional gravity traverses of the Nuba Mountains, Kordofan Province, Sudan. Journal of African Earth Sciences**,**
Vol. 5**,** 329-338.

Schandelmeier, H., Richer, A., Harms, U., Abdel-Rahman, E.M., 1990. Lithology and structure of the late Proterozoic Jebel Rahib fold-and-thrust belt (SW Sudan). Berliner Geowissen Abher (A) 120.1, 15–30.

Schandelmeier, H., Richter, A., Harms, U., 1987. Proterozoic deformation of the East Sahara Craton in southeast Libya, south Egypt and north Sudan. Tectonophysics Vol. 140, 233–246.

Shaddad, M. Z**.,** Kropachev, S. M. and Khalil, B. E., 1979. Regional geological setting of the Nuba Mountains. Geological Survey of Egypt Ann & Reports**.** Vol. 9, 446-454.

Steiner L. 1987., The Nuba ophiolite and its geologic setting. In: Matheis, G. & Schandelmeier (e,d Hs) . Current research in African earth science**.** Extended Abstracts, 14th Colloquium of African Geology, Berlin West, 101-104.

Stern, R. J. and Abdelsalam, M.G., 1998. Formation of Juvenile Continental Crust in the Arabian-Nubian shield: Evidence from Granitic rocks of the Nakasib Suture, NE Sudan. Geologische Rundschau. Vol. 87, 150-160.

Stern, R. J., Johnson, P. R., Kröner, A., and Yibas, B., 2004. Neoproterozoic Ophiolites of the Arabian-Nubian Shield, in Kusky, T., editor, Precambrian Ophiolites and Related Rocks: Elsevier, Developments in Precambrian Geology, Vol. 13, 95–128, doi: 10.1016/S0166-2635(04)13003-X.

Sun, S. S. and Mc Donough W. F., 1989. Chemical and isotopic systematics of oceanic basalts: implications for mantle composition and processes. Geological Society, London, tectonic fingerprinting of ancient oceanic lithosphere. Geological Society of America Bulletin. Vol. 123; no. 3/4; 387– 411.

Tollstrup, D. L. and Gill, J. B., 2005. Hafnium systematics of the Mariana arc: Evidence for sediment melt and residual phases. Geology. Vol. 33 no. 9, 737-740.

Vail, J**.** R., 1973. Outline of the geology of the Nuba Mountains and vicinity southern Kordofan Province, Sudan. Bulletin of the Geological and mineral Resources Authority of the Sudan, No. 23

Vail, J. R. 1983. Pan-African crustal accretion in northeast African. Journal of African Earth Sciences. Vol. 1, 285-294.

Vail, J. R. 1985. Pan-African (late Precambrian) tectonic terranes and reconstruction of the Arabian-Nubian Shield. Geology, Vol. 13**,** 839-842.

Vail, J. R., 1990. Geochronology of the Sudan. Overseas Geology and Mineral Resources. no. 66.

Wilson, M., 1989. Igneous Petrogenesis: A global tectonic approach: London,Unwin Hyman, 466 p.